NATIONAL ADVISORY COMMITTEE FOR AERONAUTICS

TECHNICAL NOTE

No. 947

STUDIES OF BLADE SHANK FORM AND PITCH DISTRIBUTION FOR CONSTANT-SPEED PROPELLERS

By Elliott G. Reid
Stanford University

Washington
January 1945

NATIONAL ADVISORY COMMITTEE FOR AERONAUTICS

TECHNICAL NOTE NO. 947

STUDIES OF BLADE SHANK FORM AND PITCH DISTRIBUTION FOR CONSTANT-SPEED PROPELLERS

By Elliott G. Reid

SUMMARY

An experimental investigation of the influences of blade shank form and pitch distribution upon the aerodynamic characteristics of constant-speed propellers has been carried out at Stanford University.

It was found that the replacement of round blade shanks by faired ones produced substantial improvements of efficiency which increased with the advance ratio. Peak efficiencies were slightly augmented by the use of unusually thin shank profiles but at the cost of serious impairment of the characteristics for reduced advance ratios; the latter effect is ascribed to the stalling characteristics of the thin profiles. It was also found that objectionable discontinuities of performance occurred when the pitch angles of exposed shank elements exceeded 90°.

Analysis of the characteristics of models with systematically related distributions of both uniform and nonuniform design pitch revealed that uniformity of the angles of attack of the blade elements is the best criterion of efficiency in unstalled operation. The test results indicate that this requirement is most nearly satisfied over a wide range of operating conditions by the pitch distribution defined by a blade twist curve which is the envelope of the twist curves for all blades of uniform design pitch. It is believed that the roots of such blades should be washed out if they are to operate in the presence of substantial body interference.

In an appended note on the selection of propellers, special attention is given to the effects of overloading.

INTRODUCTION

The necessity of selecting a pitch ratio appropriate to the anticipated operating conditions was indicated by the earliest systematic experiments made on aircraft propellers. However, the first tests of an adjustable-pitch propeller (reference 1) demonstrated that, within the limited range then investigated, optimum efficiency could be closely approached by simply rotating blades of relatively small uniform design pitch to angles larger or smaller than those for which they had been designed. Some subsequent studies of controllable propellers (e.g., references 2 and 3) have indicated the desirability of increasing the design pitch ratio, particularly for operation at large values of the advance ratio, but contradictory evidence will be found in reference 4. The advent of the constant-speed propeller and the continuous improvement of airplane performance with engines of increased power have now so complicated and extended the operating conditions as to necessitate that the influences of pitch distribution be systematically re-examined from the viewpoint of current practice.

When the first adjustable metal blades were developed, structural considerations led to the substitution of circular blade shanks for the previously used ones of airfoil profile. The advantages of adjustability and of thinner profiles at the outer radii so outweighed the disadvantages of round shanks that blades of such form were eagerly accepted and still have wide use despite the aerodynamic crudity of their inner sections. Recently, auxiliary "cuffs" and shanks of airfoil profile have had limited use in an effort to suppress this source of inefficiency, but conflicting flight test reports and the lack of comprehensive laboratory data have left some doubt of the practical value of such refinements.

The present investigation was undertaken in an effort to clarify both of the questions outlined in the preceding paragraphs. The influences of blade root form were studied by testing model propellers with round shanks, similar models equipped with replicas of streamline cuffs adequate for the enclosure of such shanks, and still other models similar to the first except for the use of relatively thin airfoil profiles for the shank sections. The question of pitch distribution was investigated by testing two families of models, both of which have thin shanks of airfoil profile. The first, of the uniform pitch type, have design blade

angles which range from 24° to 60° at 0.75 tip radius. The second group consists of three sets of blades which incorporate as many progressive departures from uniformity of design pitch and one set in which washed-out roots are combined with outer sections of uniform pitch. The tests were made in the absence of substantial body interference, and the same small spinner was used to enclose all model hubs.

This investigation, conducted at Stanford University, was sponsored by, and conducted with financial assistance from, the National Advisory Committee for Aeronautics.

SYMBOLS

D	diameter, feet
R	tip radius, feet
A	disk area (πR^2), square feet
B	number of blades
r	radius of element, feet
b	chord of element, feet
h	maximum thickness of element, feet
ρ	air density, slugs per cubic foot
V	airspeed, feet per second
n	rotative speed, revolutions per second
V/nD	advance ratio (replaced by J in figs. D and E)
P	power input, foot-pounds per second
T	thrust, pounds
C_P	power coefficient ($P/\rho n^3 D^5$)
C_T	thrust coefficient ($T/\rho n^2 D^4$)
η	efficiency ($C_T V/C_P nD$)

η_i ideal efficiency ($\eta_i^2/1-\eta_i = 2\ \rho\ AV^2/T$)

C_{PT} thrust-power coefficient (ηC_p)

β pitch angle of element, degrees (reference-chord line)

β' pitch angle of element, degrees (reference-lift axis)

β'_T pitch angle of tip element, degrees (reference-lift axis)

ϕ effective helix angle $\left(\tan^{-1} \frac{V}{2\pi rn}\right)$, degrees

α angle of attack ($\phi - \beta'$), degrees (?)

$\Delta\alpha$ range of variation of angle of attack ($\alpha_{max} - \alpha_{min}$), degrees. (Elements between $r/R = 0.15$ and $r/R = 0.95$.)

MODELS AND APPARATUS

The model propellers used for this investigation incorporated 13 different forms of adjustable-pitch duralumin blades. All models were of 33.6 inches diameter and were equipped with 0.15D spinners of the form illustrated in figure A. The closely fitted masks which covered the spinner apertures may be seen in this photograph and attention is called to the absence of body interference.

Four-blade models were utilized for the study of blade shank form because four suitable models of this type were already available. Since they previously had been tested in combination with a wing-nacelle model, the construction of two new four-blade models made it possible to cover the range of blade shank forms desired for the present experiments and, at the same time, to determine the characteristics of the existing models in the absence of body interference. On the other hand, economy dictated the use of three-blade models for the study of pitch distribution.

The principal design characteristics of the various blade forms are presented in figures 1 to 6. Figures B and C are photographs of representative members of the group. Before enumerating the distinguishing features of these

models, it may be well to call attention to the following common characteristics: With exception of Model P, the prototype which has round shanks, all the models represent propellers the blade shanks of which are enclosed by cuffs, or are equipped with fairings, of airfoil profile. Moreover, the profiles and plan forms of the exposed portions of these blades - that is, the portions outboard of the cuffs or fairings - are, with negligible exceptions, identical with those of Model P. The blade widths and thicknesses will be found in figure 1. All the blades have NACA 16-series profiles between the tip and the station r/R = 0.785. Between this station and the outer limits of the cuffs, a transition to a modified Clark Y profile is effected. Sections of the Clark Y family are retained for the cuffs of Models P_C, P_{CH}, and P_{CS}; in all other models, a transition back to NACA 16-series profiles occurs within the length of the cuff or root fairing. In both of these groups, the profiles of the root sections are of symmetrical, although not identical, form.

Six models, the design blade angle curves of which will be found in figure 2, were used for the study of blade shank form. They have the following distinctive characteristics:

Model P.- A conventional type blade of uniform geometric design pitch ($\beta_{0.75R} = 24^\circ$) with relatively wide tip and so-called round shank. Attention is called to the measurement of β with reference to the nominal chord line and to the fact that degeneration of the airfoil profile into a circular section is complete only at the innermost section of the blade. (See figs. B, C, and 1.)

Model P_C represents Model P equipped with a cuff of Clark Y profile; the geometric pitch of the cuff is the same as that of the outer portion of the blade.

Model P_{CH} represents Model P equipped with a refined Clark Y cuff which has smaller radial and chordwise dimensions than those of P_C and incorporates a washout of 12°. (Note: Washout specified is that at the spinner surface.)

Model P_{CS} differs from P_{CH} only in pitch distribution; the outer blade angles differ very slightly (fig. 2) but the cuff washout is 16° in this case.

Model P_{C1} represents a blade of the same outer plan form and profiles as in P, but with larger design pitch ($\beta_{0.75R} = 30^\circ$) and a faired shank of unusually small thickness. (See fig. 1.)

Model P_{C2} is identical with P_{C1} except for a washout of 10° in the faired shank.

The eight models tested to determine the influences of pitch distribution incorporate the following features: U-Series (Models U-24, U-36, U-48, and U-60). All these blades have plan forms and profiles identical with those of P_{C1} and P_{C2}; their blade angle curves are shown in figure 3. In this case the blade angles are those measured with reference to the lift axes or "no lift lines" of the profiles and are therefore designated by β'. The design pitch of each of these blades is uniform in the true aerodynamic, rather than the arbitrary geometric, sense; that is, the relationship

$$P = 2\pi r \tan \beta' = \text{constant}$$

is satisfied for all values of r. The numerical designations of the U models are simply the design values of β' (in deg) at $r/R = 0.75$.

Since the only consequential result of changing the design pitch of the blades of a controllable or constant-speed propeller is to alter the twist, or variation of blade angle between root and tip, the significant differences between such blades as those of the U-series can best be illustrated by comparison of their twist curves. Vertical displacement of the curves of figure 3 by such amounts as to reduce the tip blade angle β'_T to zero in each case yields the interesting result shown in figure 4.* The small order of the differences between the angles of twist for those blades the design pitches of which differ so widely is, perhaps, less surprising than the fact that the twist curves of uniform-pitch propellers appear to define an envelope. Investigation reveals that the equation of this envelope is

$$\beta' - \beta'_T = \cot^{-1}\sqrt{r/R} - \tan^{-1}\sqrt{r/R} \qquad (1)$$

*Similar curves for models of the P-series are shown in fig. 5; the irregularities apparent there result from the common design practice of basing pitch calculations upon values of β rather than β'.

This relationship was utilized in the design of the E-Series (Models 0.8E, 0.6E, and 0.4E). These models differ from those of the U-series only in that they are of nonuniform design pitch; their twist curves appear in figure 6. The ordinates of these curves were derived from those of the envelope curve by multiplying the latter, successively, by 0.8, 0.6, and 0.4. The "fractional envelope" models which incorporate these twist curves are correspondingly designated.

Model P_{C2}.- Tests of a three-blade model of this type were added to the original program for the study of pitch distribution.

The experimental work was conducted in the 7.5-foot wind tunnel of the Guggenheim Aeronautic Laboratory of Stanford University. Descriptions of this tunnel and of the propeller dynamometer will be found in reference 5. The only departure from previous practice was the reduction of the diameter of the dynamometer shroud to that of the spinner; this was done to eliminate the stepped contour associated with the previous telescoping arrangement and had the desirable effect of reducing the difference between the pressure on the back of the spinner and the static pressure of the air stream.

TESTS AND TECHNIQUE

The experiments were conducted in accordance with established Stanford practice, which is to test model propellers at fixed rotative speeds and to vary the advance ratio by altering the airspeed. Listed below are the blade angles* and corresponding rotative speeds at which each model was tested in the course of the present investigation:

Four-blade models:	P,	P_C,	P_{CH},	P_{CS},	P_{C1},	P_{C2}
$\beta_{0.75R}$ (deg)	20	30	40	50	60	
Rotative speed, rpm	2100	1740	1314	996	744	
Three-blade models:	U-series, E-series, and P_{C2}.					
$\beta_{0.75R}$ (deg)	12	24	36	48	60	
Rotative speed, rpm	2100	2100	1470	1056	744	

*Nominal angles, β; reference - arbitrary chord line.

The airspeeds ranged from approximately 90 mph to the lowest values at which reliable observations of dynamic pressure could be made.

To insure against errors of blade setting, observation or computation, two tests were made on each model at each pitch setting. Upon completion of the first test of each pair, the model was removed from the dynamometer and the blade angles were carefully checked; upon completion of the second test, the procedure was repeated. In the check run, observations were made at airspeeds so chosen that the corresponding values of V/nD were staggered with respect to those of the original test. Data were rejected and experiments repeated in all instances in which the results of the paired tests exhibited any substantial or consistent difference.

The data observed at each airspeed were thrust, torque, dynamic pressure, rotative speed, barometric pressure, wet- and dry-bulb temperatures, and pressure on the back of the spinner. The number of such sets of simultaneous observations made during a single test varied from 11, when $\beta_{0.75R} = 12^\circ$, to 22, in the case of the 60° setting.

REDUCTION OF DATA

The experimental data have been reduced to the usual nondimensional forms

$$C_P = P/\rho n^3 D^5 \qquad C_T = T/\rho n^2 D^4$$

For the calculation of C_T, the measured thrusts were corrected to the values which would have prevailed had the pressure on the back of the spinner been equal to the static pressure of the air stream. These spinner thrust corrections were determined and applied as a routine precaution which has been found particularly important when large spinners are used; in the present instance, their effects upon the final results were inconsequential.

Efficiencies were calculated in accordance with the relationship

$$\eta = (C_T/C_P)(V/nD)$$

For the fairing of the peaks of the efficiency curves, additional guidance was furnished by auxiliary efficiency values which were computed by use of the coordinates of C_P and C_T against V/nD curves as faired on large-scale Cartesian charts.

Some few data have been reduced to the form of thrust-power coefficients. The equation

$$C_{PT} = \eta C_P$$

defines the relationship between the thrust (or effective) and ordinary (or brake) power coefficients.

RESULTS

For purposes of illustration, complete numerical data for one of the 14 models which were studied are included in this report. These test results, which pertain to Model U-36, will be found in tables I to V; similar data for the other models, presented herein only in graphical form, may be obtained on loan from the Office of Aeronautical Intelligence, NACA, Washington, D. C.

The test results were originally plotted in the form illustrated by figure 7. This is a photograph of a large chart the logarithmic scales of which have moduli of 10 inches. The example chosen for reproduction contains all the data included in tables I to V. In figures 8 to 21, the characteristics of all 14 models are reproduced from tracings of charts similar to figure 7.

These primary charts depict, of course, the characteristics of propellers with fixed pitch settings and are, consequently, of little direct use for analysis of the merits of the various types of blade under the conditions of constant-speed operation. It has, therefore, been necessary to devise new graphical methods of comparison in order that the results of these tests may be viewed from the standpoint of operation at constant values of C_P rather than that of fixed blade angles. Charts of form appropriate to this purpose have been derived from figures 8 to 21; their preparation will be outlined as they are referred to in the following section.

DISCUSSION

Blade Shank Form

Perhaps the most important fact brought to light by the study of blade shank form is the marked superiority of faired shanks over round ones. This will become apparent if an inspection is made first of the efficiency curves of figure 8, which refer to the round-shank prototype, Model P, and then the corresponding curves of figures 9 to 13, which illustrate the characteristics of those with faired shanks, Models P_C, P_{CH}, P_{CS}, P_{C1}, and P_{C2}.

Detailed examination of these figures will reveal that the effect of fairing the blade shanks is to augment both the power and thrust coefficients which correspond to given pitch settings. The improvement of efficiency is, of course, the result of the greater proportional increase of thrust than of power. This quantitative relationship may be readily confirmed by reference to the logarithmic charts (figs. 8 to 13) because, in this form of plotting, proportionate changes of unequal ordinates are characterized by equal vertical displacements of points. It will be observed that the differences between the characteristics of blades with round and faired shanks become progressively greater as the pitch is increased.

Envelope efficiency curves, traced from figures 8 to 13, are shown in figures 22 and 23. There it may be seen that the improvement of peak efficiency due to fairing increases with the advance ratio and attains a value of approximately one-seventh, or 10 percent, when $V/nD = 3.0$. It will be noted, however, that the envelope curves for the models with various forms of faired shanks differ so slightly that it has been necessary to separate them into two groups in order that they may be distinguished at all. Despite this approximate coincidence of the envelope efficiency curves, it is quite unwarranted to conclude that variation of the form of shank fairing has a negligible effect upon the characteristics of a propeller. These less obvious differences are not readily distinguishable in charts which portray the characteristics of blades with fixed pitch settings; to expose them, it has been necessary to develop the "constant-speed efficiency chart" which is described below.

The characteristic which distinguishes the operation of a constant-speed propeller is that at a given altitude and under specific conditions of engine operation (i.e., fixed values of imp and rpm and, hence, bhp), the power coefficient C_p remains constant while the airspeed and advance ratio may vary throughout the take-off, climb, level flight, and diving regimes. It thus appears that the relative merits of different forms of propeller blades intended for constant-speed operation can be fairly appraised only by comparing the efficiencies which they attain while operating at equal values of the power coefficient and over wide ranges of V/nD. The maintenance of a constant-power coefficient under such conditions implies, of course, corresponding variations of the pitch setting; this is accomplished in flight by the action of the constant-speed governor but it can be effectively accomplished in the laboratory by deriving appropriate curves from the results obtained by testing models at several fixed pitch settings.

The method of preparing such curves is illustrated by figure 27. Experimental results are represented by curves of C_p against V/nD and contours of equal efficiency. By drawing horizontal lines across these contours at selected values of C_p, the values of V/nD at which the "contour values" of efficiency will be attained are determined by the positions of the intersections. Thus the curves designated "η, C_p = constant" are constructed simply by plotting the contour values of efficiency as ordinates at the abscissas of the corresponding intersections. Each of these curves therefore defines the efficiency which will be attained when the pitch is so adjusted as to maintain C_p at a constant value while the advance ratio varies.

The constant-speed efficiency curves for the four models which have thick shanks are compared in figure 28. In the upper chart, the characteristics of the round-shank blades, Model P, are compared with those of the blades which incorporate the primitive thick, wide cuffs, Model P_C. It is now clearly evident that the improvement of efficiency under optimum (envelope) conditions is accompanied by substantial improvements under all other operating conditions included in these tests. The reader's attention is called to the nonuniformity of the improvement at various values of C_p and V/nD.

Since all the models with faired shanks excel Model P, the characteristics of Model P_C have been selected as the basis for subsequent comparisons. Thus, in the middle chart of figure 28, it is seen that the curves for Model P_{CH} superimposed upon those of Model P_C. In this case, the only differences of any consequence are confined to the curves for $C_P = 0.5$ and 0.7. As previously indicated by the envelope curves, Model P_{CH} develops slightly higher peak efficiencies at large values of V/nD, but this is offset somewhat by the superiority of Model P_C at the reduced values of V/nD* which would be utilized in climbing flight when $C_P = 0.5$. Attention is also called to the discontinuity in the efficiency curve of Model P_C for $C_P = 0.7$; this undesirable characteristic constitutes an ample reason for rejecting Model P_C in favor of Model P_{CH} which reproduces practically all the desirable characteristics of the former.

Although the origin of the discontinuities which characterize the curves for Model P_C (with $C_P = 0.7$ or $\beta_{0.75R} = 60^\circ$) cannot be positively identified in the absence of wake survey data, there can be little doubt that the large angle of twist incorporated in this blade design is the basic cause of the irregularity. When the blades with faired shanks are set to 60° at 0.75R, the pitch angles of the elements at the surface of the spinner are

Model	P_C	P_{CH}	P_{CS}	P_{C1}	P_{C2}
β (at spinner, deg)	102	90	86	99	91

Examination of the 60° C_T curve of figures 9 to 13 will reveal that a marked effect of increasing the angle of twist is to depress that portion of the C_T curve which lies to the left of the peak. This is particularly evident in the case of Models P_{C1} and P_{C2}, which differ only in cuff pitch angles. A considerable part of this reduction of thrust is believed to be the result of stalling of the shank elements and it would appear obvious that the adverse effect of rearward rotation of the resultant force vectors must increase

*The phrase "at reduced values of V/nD" will be used, hereafter, to designate the ranges of advance ratio below the values at which peak efficiencies occur.

as the blade angles of the shank elements progress beyond 90°. In the case of Model P_C, the stalling of the shank is probably delayed by the increased induced velocities arising from the greater cuff width, but it is interesting to note that when the stall does occur, C_T drops to a level as low as that attained by the other highly twisted blade, Model P_{C1}. These considerations indicate the desirability of avoiding excessive angles in the design of cuffs for blades which are to operate at high pitch settings.

Resuming, now, comparison of the various types of blade, the characteristics of Model P_{CS} will be found superimposed upon those of Model P_C in the lower chart of figure 28. The inferiority of Model P_{CS}, at all but the lowest power coefficient, is quite apparent upon inspection of the curves. Since the only difference between the blades of Models P_{CS} and P_{CH} was presumed to be the slight divergence between their twist curves which is illustrated by figure 5, the inferiority of the performance of Model P_{CS} seemed rather surprising until it was discovered that, through some error of manufacture, the cuff profiles of Model P_{CS} deviated seriously from the specified forms. This fact is believed to explain most of the difference between the characteristics of Models P_{CS} and P_{CH}.

The characteristics of Models P_{C1} and P_{C2}, which have thin faired shanks and a somewhat larger design pitch than the thick-cuff models, are compared with those of Model P_C in figure 29. Close inspection shows that Model P_{C1} is inconsequentially superior to Model P_C under any condition; whereas Model P_C is by far the better under the conditions for climb at moderate and high powers. The beneficial effects of reducing the pitch angles of the faired shank profiles is shown by the curves for Model P_{C2}. It is noteworthy that efficiency is improved very considerably for the larger values of C_P and reduced but little when C_P is small. However, even the Model P_{C2} does attain efficiencies which, at large values of V/nD, slightly exceed those of Model P_{CH}, the greater superiority of Model P_{CH} at reduced values of V/nD would appear to outweigh the limited high-speed advantage of Model P_{C2}. In this connection, it should

be remembered that V_{max} varies approximately with $\eta^{1/3}$; whereas the rate of climb varies in larger proportion than does η.

The differences between the characteristics of the blades with thick and thin faired shanks appear to be consistent with the properties of the shank profiles. The 16-series profiles used for the thin shanks are known to be characterized by comparatively small values of C_{Lmax} as well as C_{Dmin}. The influences of C_{Dmin} would be expected to be beneficial when the shank elements operate at the small or moderate angles of attack at which maximum efficiencies are attained. On the other hand, as V/nD is reduced and the angles of attack increased, it is to be expected that flow separation from the thin 16-series shanks will occur before the thicker Clark Y profiles stall, and that the efficiencies of the thin-cuff models will therefore be inferior at reduced values of V/nD.

It is emphasized that the foregoing explanation does not imply that thick cuffs are inherently superior to thin ones. On the contrary, there is every reason to believe that for operation at high Mach numbers, thickness should be minimized insofar as is compatible with adequate strength and reasonably large maximum lift coefficients.

Before proceeding to the discussion of the other phase of the investigation, the principal findings of the study of blade shank form are summarized herewith:

1. The efficiencies of constant-speed propellers can be materially improved by the substitution of faired shanks for round ones.

2. The design pitch angles of the shank sections should be so chosen that the operating pitch angles of the elements outside of the spinner will not substantially exceed 90°.

3. The use of shank profiles characterized by small values of C_{Lmax} appears undesirable.

Pitch Distribution

Uniform pitch.- The fixed blade angle characteristics of the four models of the U-series, illustrated by figures

14 to 17, are as remarkable for features of close resemblance as they are for divergences. One rather surprising resemblance is seen in the power coefficient curves; it is apparent that as long as the design pitch ratio is uniform, its value may be varied between wide limits without seriously influencing the forms or positions of the curves of C_p against V/nD which correspond to given blade settings at 0.75R. Equally evident, however, are the marked differences of form exhibited by the thrust coefficient curves for the four models. But even in this case, it will be noted that the major differences are confined to those portions of the curves which represent partially or fully stalled operation of the blades. Examination will show that as the design pitch angle is increased from 36° to 60° - that is, as the angle of twist is reduced - the valleys which characterize the low V/nD sections of the thrust curves for large blade angles are progressively filled up.

These varied characteristics combine to yield efficiency curves which differ somewhat in form but define envelopes which deviate by the remarkably small amounts shown in figure 24. Interesting features of these curves are the relatively high efficiency of Model U-60 at both extremes of the V/nD range, its uniquely low efficiency in the middle range, the inefficiency of Model U-48 at small values of V/nD, and the apparent tendency for the models of this group to assume, at very large advance ratios, an order of merit identical with the order of magnitude of their design pitch ratios.

When the constant-speed efficiency curves of figure 30 are compared, it is apparent that Model U-24 is slightly, but clearly, superior to the other three members of the U-series under a large majority of operating conditions. To be sure, Model U-60 excels all the others within a limited range of the advance ratio when the power coefficient is large and Model U-48 attains slightly higher peak efficiencies at values of V/nD between 3 and 3.5, but it appears that these are the only conditions under which the curves for Model U-24 are not either equal or superior to those of all the other uniform pitch models.

Nonuniform pitch.- A considerable degree of resemblance is to be seen between the fixed-blade-angle characteristics of the uniform pitch (U-series) and fractional envelope (E-series) blades. Reference to figures 18 to 20 reveals that as the total angle of twist within the length of the

blade is reduced in the transformation from Model 0.8E to Model 0.4E (fig. 6), the aerodynamic characteristics are altered in a manner which resembles that previously cited in connection with the somewhat similar reduction of twist which occurred as the uniform design pitch was increased. (See fig. 4.) The similarity is most noticeable in the progressive filling up of the deep valleys just to the left of the peaks of the thrust coefficient curves for $\beta_{0.75R} = 60^\circ$ and (fig. 31) in the straightening of the rising portions of the efficiency curves and lowering of their peaks. As the twist curve for the fourth set of nonuniform pitch blades, Model $P_{C2}(3)$*, is more nearly similar to that for Model 0.8E than to those of the other members of the E-series; it is not surprising that comparison of figures 20 and 21 reveals relatively small differences between their characteristics for equal blade settings.

It will be seen in figure 25 that the envelope efficiency curves for the nonuniform pitch propellers are much more widely separated than those for the uniform pitch group. The progressive depression of the envelope with reduction of the angle of twist incorporated in the blade is consistent with the results of the U-series tests. The fact that the envelope for Model 0.4E is even lower than that for Model U-60 is easily understood when the ordinates of their twist curves are compared. (See figs. 4 and 6.) The inferiority of the envelope efficiency of Model $P_{C2}(3)$ at low values of V/nD is ascribed to the excessive twist in the outer portions of the blades of this type; the same influence is discernible in the envelopes for the blades of uniform pitch.

The constant-speed efficiency curves of figure 31 (upper and middle charts) reveal that the effect of reducing blade twist is to augment the efficiencies developed at low values of V/nD, particularly when C_p is large, but at the expense of serious efficiency reductions in the range of advance ratio which would be utilized for normal climbing and level flight. In other words, the curves of η against V/nD for given values of C_p are "straightened" - that is, the characteristic concavity of the rising slope is eliminated by elevation of the lower portions and depression of the upper ones. However, if the curves for equal values of

*(3) indicates three blades, as in other models of U- and E-series.

C_p are compared, it will be seen that Model 0.8E is more efficient than either Model 0.6E or 0.4E at all values of V/nD greater than 0.6 (V/nD) for maximum efficiency. It thus appears that blades which incorporate relatively small angles of twist are, under normal conditions of flight, inferior to otherwise similar blades the twist curves of which more closely approach the envelope form. It will be seen, also, that selection of one of the slightly twisted blades with the object of improving take-off at large values of C_p would entail disproportionately large sacrifices of normal flight performance.

The lower chart of figure 31 shows that nonuniform pitch blades of the type P_{C2} are inferior to those of Model 0.8E under all conditions in which their characteristics differ appreciably. Tests of Model $P_{C2}(3)$ were added to the original program for the investigation of pitch distribution when it was found that the four-blade model of this type developed higher efficiencies than the uniform pitch type P_{C1}. However, figure 31 conclusively demonstrates that mere reduction of the pitch of the inner portion of a uniform pitch blade ($\beta'_{0.75R} = 33^\circ$, approx.) does not result in efficiencies quite as great as those obtained with blades of the type 0.8E.

Comparison of uniform and nonuniform pitch.- It has been pointed out that, when viewed from the standpoint of constant-speed operation, Models U-24 and 0.8E are, respectively, the best of the uniform and nonuniform pitch types tested. The characteristics of these two models will now be compared, and an effort will be made to determine the sources of their superiority.

The constant-speed efficiency curves for Model 0.8E are superimposed upon those of Model U-24 in figure 32. While neither set of curves is superior to the other under all conditions, it is clear that Model 0.8E attains the higher efficiencies at both extremes of the V/nD range (see envelopes, fig. 26) and, at intermediate advance ratios, its superiority at high power coefficients appears at least to balance its inferiority at low ones. It is therefore concluded that the pitch distribution incorporated in Model 0.8E is slightly better suited to the conditions of constant-speed operation in the absence of body interference than are those of any of the other models tested. The relatively slight susceptibility to body interference of blades with

washed-out roots (reference 6) makes it reasonable to assume that this superiority would be augmented in the presence of an interfering body.

As a preliminary step toward isolation of the characteristics of pitch distribution which underlie the superiority of Models U-24 and 0.8E, it may be of interest to compare the efficiencies actually attained by models of large and small design pitch with the ideal values predicted by momentum theory. Previous comparisons of this kind have involved the preparation of an individual chart for each value of the power coefficient because the ideal efficiency depends upon both C_p and V/nD as indicated by the equation

$$\frac{\eta^a}{1-\eta} = \left[\frac{2\rho AV^2}{T} = \frac{\pi\rho V^3 D^2}{2\eta P} =\right] \frac{\pi}{2\eta\ C_p}\left(\frac{V}{nD}\right)^3 \qquad (2)$$

This complication can be eliminated, however, and a much more comprehensive comparison can be made in a single chart when it is recognized that the ideal efficiency is completely determined by the value of the parameter $(V/nD)\ C_p^{-1/3}$ - that is,

$$(V/nD)\ C_p^{-1/3} = \eta\ (2/\pi(1-\eta))^{1/3} \qquad (3)$$

Thus, in figure 33, use of $(V/nD)\ C_p^{-1/3}$ as the independent variable enables representation of the ideal efficiency for all values of C_p by a single curve and plotting of the actual constant-speed efficiencies to this same scale of abscissas yields a very clear illustration of the influence of C_p upon the relationship between actual and ideal efficiencies.

The actual efficiencies are seen to be of the order of 90 percent of the ideal ones throughout a wide range of advance ratio when the power coefficient is small, but as C_p increases the ideal values are closely approached only within very limited ranges. The large discrepancies which appear under the latter conditions are, of course, the consequences of stalling of major portions of the blades as the blade angles and angles of attack increase. While these curves show that blades of large and small design pitch do not attain equal fractions of the ideal efficiency under

comparable conditions, and that they exhibit very different stalling characteristics, it is apparent that, for quantitative analysis of such differences as these, information concerning the magnitude and distribution of the angles of attack will be required.

Such data have been obtained for all the models involved in the study of pitch distribution. The angle-of-attack curves which appear in figures 37 and 38 correspond to representative conditions of climbing and level flight; they were prepared as follows: The straight line designated I in figure 27 approximates the mean of the curves which connect the maximum efficiency points of the fixed-blade-angle curves of C_p against V/nD for the eight models used in the pitch investigation. The parallel line II defines values of V/nD which, at given values of C_p, are 0.6 of those for line I. Reproduction of these lines on figures 14 to 21 furnished the corresponding values of C_p and β which define the curves of figures 34 and 35. Finally, the blade angles required for the development of $C_p = 0.5$, 0.2, and 0.05 at the values of V/nD defined by lines I and II were read from figures 34 and 35. Knowledge of the blade settings, twist characteristics, and advance ratios enabled determination of the radial distribution of blade angles (β'), advance angles (ϕ), and angles of attack (α) as illustrated by figure 36. The results of these calculations are summarized graphically in figures 37 and 38; attention is called to the use of the lift axis as the reference line for measurement of the angles of attack defined by these curves.

To facilitate the establishment of a basis of correlation between efficiency and angle-of-attack distribution, the most pertinent data have been tabulated in table VI. There will be found the maximum and minimum values of the angle of attack ($0.05 < r/R < 0.95$), their difference, and the efficiency developed by each model under each of the six selected conditions of comparison: namely,

C_p	0.5	0.2	0.05
V/nD (I)	2.85	1.80	0.90
V/nD (II)	1.71	1.08	0.54

Before examining these data in detail, it may be well to call attention to one special feature of figures 37 and 38; it is that when $C_p = 0.5$ and $V/nD = 1.71$, the values

of α for all eight models substantially exceed the critical ones for normal airfoils - that is, major portions of all the blades are fully stalled. It would therefore seem prudent to exclude this condition from the present consideration until a satisfactory analysis of unstalled operation has been obtained and then to consider this one as a special case.

When the corresponding values of $\Delta\alpha$ and η for the several models are compared, one unmistakable qualitative relationship becomes apparent at once: Under each of the five conditions of unstalled operation, the model characterized by the largest value of $\Delta\alpha$ is least efficient. (Examination of figs. 37 and 38 reveals that the inner portions of these least efficient blades (Model 0.4E) operate at negative angles of attack.) It is also indicated, although not quite so clearly, that there is a general tendency for η to increase as $\Delta\alpha$ decreases.

Clear-cut evidence of the influence of $\Delta\alpha$ upon η will be found in figure 39. In the three high-speed conditions, which represent operation approximately at the peaks of the efficiency curves for $C_p = 0.5$, 0.2, and 0.05, the value of η is seen to improve continuously as $\Delta\alpha$ approaches zero. This is also true of the climbing condition, $C_p = 0.2$ and $V/nD = 1.08$, but when $C_p = 0.05$ and $V/nD = 0.54$, both $\Delta\alpha$ and η vary so slightly that the influence of $\Delta\alpha$ appears to become irregular in the case of the models of the U-series. In general, however, it is quite evident that for unstalled operation the most desirable form of pitch distribution is the one which leads to the smallest variation of the angle of attack along the blade.

Turning, now, to the special case of climb at high power ($C_p = 0.5$, $V/nD = 1.71$), an explanation must be sought of the marked superiority of the envelope type blades over those of uniform pitch. The clue is found in the curves of figures 37 and 38. The least efficient blades are characterized by large and substantially uniform angles of attack throughout the lengths of the blades; whereas the most efficient blades are those in which the angles of attack of the inner elements are much smaller than those of the outer ones. Since the outer elements of the nonuniform pitch blades attain even larger angles of attack than do the corresponding ones of the uniform pitch models, the development of greater efficiencies by the nonuniform pitch blades forces the conclusion that the beneficial effect of

maintaining continuous flow over the inner portions of these blades outweighs the adverse consequences of the associated more complete stalling of their tips.

In figure 39, identification of the points which represent the various models enables recognition of an interesting difference between the behavior of the two families of blades which have uniform and nonuniform design pitches. It will be seen that among the envelope type blades, Model 0.8E has the least, and Model 0.4E has the greatest, value of $\Delta\alpha$ under all conditions. On the other hand, the values of $\Delta\alpha$ for the uniform pitch blades do not maintain a fixed order - that is, as V/nD assumes the values 0.90, 1.80, and 2.85 - the models which exhibit the smallest values of $\Delta\alpha$ are, respectively, U-24, U-36, and U-48. The variations of $\Delta\alpha$ with V/nD for the models of the U- and E-series are illustrated by figure 40. The implications of this dissimilarity merit serious consideration in the selection of the optimum pitch distribution for constant-speed propellers which must operate over wide ranges of both C_p and V/nD.

Although the relationship exhibited by the models of the E-series in figure 39 indicates that $\Delta\alpha$ might be further reduced, and η thereby improved, by the use of blades of envelope form - that is, a "Model 1.0E" - the shifting order of merit of the models of the U-series makes it difficult to visualize the properties of intermediate members of this group. To enable reasonably accurate estimation in both cases, the data of figure 40 have been replotted in the alternative form of figure 41. From these curves, the extrapolated and interpolated values of $\Delta\alpha$ for the nonexistent Models 1.0E, U-30, and U-42 have been transferred back to figure 40 where the corresponding curves of $\Delta\alpha$ against V/nD are shown as broken lines. Triangular and arrow-shape symbols in figure 39 identify the anticipated efficiencies of such models.

The close proximity of the arrows to the maximums of the curves of η against $\Delta\alpha$, as compared with the inferior locations of the triangles of either kind, clearly indicates that: The envelope pitch distribution is superior to any uniform one for the blades of a constant-speed propeller which experiences negligible body interference.

Since the criterion of uniformity of the angles of attack leads to the foregoing conclusion, it would appear to dictate, also, the following corollary: The envelope form

of blade twist should be modified by the introduction of sufficient root washout to compensate for the local reduction of velocity when body interference is present.*

Influences of Blade Loading and Number of Blades

Although the original plan for the present investigation included no treatment of this question, the testing of models which had both three and four blades of the same form (P_{C2}) offers an opportunity to add to the meager store of existing knowledge concerning the effects of augmenting propeller solidity by increasing the number of blades.

Experimentally determined efficiencies for these two models are compared with the ideal values in figure 42. It will be observed that the experimental curves for both types closely approach the ideal one throughout a wide range of V/nD when C_p is small, but that they fall far below it everywhere outside of a very limited range when C_p becomes large. Of at least equal importance is the fact that the adverse effects of increasing C_p are much greater with three blades than with four.

Since the momentum theory predicts no change of efficiency so long as C_p and V/nD remain fixed (equation (3)), it is apparent that the advantages of the four-blade type can result only from reduction of the forces on the individual blades. The almost exclusive control of efficiency by blade loading and the absence of any consequential effect of the actual number of blades is clearly shown by figure 43. There it appears that propellers which have different numbers of blades of a common form attain practically identical fractions of the corresponding ideal efficiencies (η/η_i) when the loadings of their individual blades (C_p/B) are the same at equal values of V/nD.

This interesting relationship not only furnishes a convenient basis for prediction of the effect of altering solidity by changing the number of blades but emphasizes the far greater importance of blade loading than of disk loading at present levels of design practice. It also indicates

*The beneficial effects of so modifying blades of uniform design pitch were pointed out long ago in reference 6.

that the serious impairment of efficiency at reduced values of V/nD which results from excessive blade loading can be avoided - without appreciable penalty at large advance ratios - by increasing solidity by the addition of blades. Further discussion of this subject will be found in the appendix.

CONCLUSIONS

The investigation of blade shank form has shown that:

1. Propulsive efficiency is substantially improved by the substitution of faired blade shanks for round ones.

2. The shank sections should be so designed that the pitch angles of the exposed elements will not substantially exceed 90° under any condition of operation.

3. The use of shank profiles characterized by small values of $C_{L_{max}}$ appears undesirable.

The most important facts revealed by the study of pitch distribution are:

4. Uniformity of the angles of attack along the blade appears to be the best criterion of efficiency under conditions of unstalled operation. It also appears that later stalling of the root than the tip has a beneficial effect upon the efficiencies attained at reduced values of V/nD.

5. Blades which incorporate small angles of twist in their outer portions - that is, those of large uniform design pitch and those having small fractions of the "envelope twist" - are so inefficient under the majority of normal flight conditions as to make them unsuitable for use in constant-speed propellers.

6. Conversely, blades the twist curves of which approach the envelope form exhibit the best constant-speed performance characteristics.

7. Interpolation and extrapolation of the experimental results indicate that the envelope form of pitch distribution is superior to any other for the blades of constant-speed propellers which are to operate in the absence of

substantial body interference. It is believed that the incorporation of washout in the roots of such blades would prove beneficial when the velocities near the hub are reduced by interference.

Analysis of the effects of blade loading shows that:

8. Excessive blade loading has severe adverse effects upon efficiency at reduced advance ratios.

9. At equal advance ratios, propellers which have different numbers of blades of a common form attain substantially equal fractions of the corresponding ideal efficiencies when the loadings of their individual blades are equal.

Stanford University,
Stanford University, Calif., March 20, 1943.

REFERENCES

1. Durand, William F., and Lesley, E. P.: Experimental Research on Air Propellers. II. NACA Rep. No. 30, 1919.

2. McCoy, H. M.: A Discussion of Propeller Efficiency. Jour. Aero. Sci., vol. 6, no. 6, April 1939, pp. 227-234.

3. Theodorsen, Theodore, Stickle, George W., and Brevoort, M. J.: Characteristics of Six Propellers Including the High-Speed Range. NACA Rep. No. 594, 1937.

4. Biermann, David, and Hartman, Edwin P.: Tests of Two Full-Scale Propellers with Different Pitch Distributions, at Blade Angles up to 60°. NACA Rep. 658, 1939.

5. Lesley, E. P.: Tandem Air Propellers. NACA TN No. 689, 1939.

6. Lesley, E. P., and Reid, Elliott G.: Tests of Five Metal Model Propellers with Various Pitch Distributions in a Free Wind Stream and in Combination with a Model VE-7 Fuselage. NACA Rep. No. 326, 1929.

7. Lock, C. N. H., and Bateman, H.: Wind Tunnel Tests of High Pitch Airscrews. Part II. Variations of Blade Width and Blade Section. R. & M. No. 1729, British A.R.C., 1936.

8. Hartman, Edwin P., and Biermann, David: The Aerodynamic Characteristics of Four Full-Scale Propellers Having Different Plan Forms. NACA Rep. No. 643, 1938.

APPENDIX

NOTE ON THE SELECTION OF PROPELLERS WITH SPECIAL REFERENCE TO OVERLOADING

It is believed that the take-off, climb, and ceiling characteristics of many inherently fine airplanes are being needlessly impaired by the overloading of their propellers under those conditions. The term "overloading" is used here to denote the operation of propellers with blades of normal width at excessively large values of power coefficient per blade (C_p/B); the importance of this parameter is indicated by the fact that as its value increases, thrust horsepower available for propulsion ceases to be even approximately proportional to brake horsepower and may actually diminish as the power input is further augmented.

The existence of such a "regime of diminishing returns" was pointed out by the writer in 1940 but, since that analysis was appended to a still-confidential report, the objectives of the present discussion are to promote more general recognition and understanding of the phenomenon of overloading and to discuss means for avoiding its adverse effects.

To facilitate visualization of the efficiency of a constant-speed propeller as a continuous function of the two independent variables, C_p and V/nD, the curves of figure 27 - which pertain to Model U-36 - have been embodied in the three-dimensional efficiency model illustrated by figure D. In this model, the vertical sides of the laminated block represent the limits of the experimental data; within those limits, efficiency is represented by the height of the block. The solid lines on the surface define the relationships

between C_p and V/nD for various fixed pitch setting and the dot-and-dash line connects the highest points of the constant-C_p sections.

It will be seen that the surface of this model is continuously convex in the region in which C_p is small but that concavity of the low V/nD flank appears at intermediate values and becomes very marked at values of C_p greater than 0.2. This will be recognized as the previously discussed effect of increasing the blade loading. Now, since efficiency at large values of C_p is seriously reduced everywhere outside of a narrow range of V/nD, it appears that when brake horsepower input (proportional to C_p) is increased while V/nD remains constant, the thrust horsepower available for propulsion (proportional to ηC_p) may increase in much smaller proportion if, indeed, it increases at all. However, as the effect of the variation of efficiency upon the relationship between brake and thrust powers cannot readily be visualized by inspection of the simple efficiency model, the supplementary thrust-power coefficient model shown in figure E has been constructed to illustrate this most important characteristic of a typical constant-speed propeller.

In figure E, the ordinates of the model represent the effective- or thrust-power coefficient, $C_{pT} = \eta C_p$, as a function of C_p and V/nD. Since the coordinates of this model are also logarithmic, the profiles of its constant-C_p sections (fig. 45) are identical in form with the corresponding ones of the efficiency model (fig. 27). Even more significant, however, is the fact that these curves are identical in form and orientation with the logarithmic curves of available thrust horsepower against velocity which correspond to the same values of C_p.

From the standpoint of overloading, the most significant features of the shape of the thrust-power model are the relatively small height of its left rear portion and the presence of a definite transverse crest which is identified by the dashed line designated $\partial(\eta C_p)/\partial C_p = 0$ in figure E. Although the existence of this crest may be confirmed by examination of the curves of figure 45, it is not unmistakably apparent in figure E; visualization will therefore be

facilitated by inspection of figure F, which is a photograph made while the model was illuminated by a beam of light the rays of which were parallel to the C_p axis. Here it may be seen that all the surface behind the dashed "crest line" is in total darkness while the meager illumination of adjacent regions indicate that very small positive values of $\partial(\eta C_p)/\partial C_p$ prevail there. This partial shadow identifies the regime of severe overloading; whereas the total absence of surface illumination indicates what may be termed saturation.

The potential performance of an airplane obviously will not be realized if the values of V/nD and C_p which define the operating conditions for its propeller correspond to a point within the shadowed area of the model's surface. In fact, operating conditions which involve crossing the crest line impose an impenetrable "propeller ceiling" upon performance - that is, they place a definite limit upon the thrust horsepower which may be developed even though the engine power be indefinitely increased.

The projection of the crest line for Model U-36 upon the $V/nD, C_p$ plane is shown in figure 46, along with similar curves for the other models of uniform design pitch. Corresponding curves for the nonuniform-pitch models are presented in figure 47. It may be correctly inferred from the relation of the shadow fringe, in figure F, to the crest line, in figure E, that although the best of the models tested (0.8E and U-24) are capable of efficient operation, within limited ranges of V/nD, at values of C_p as great as 0.6 to 0.7, it would be a mistake to utilize them at power coefficients much greater than 0.2 if $1.0 < V/nD < 1.5$, because close approach to the crest line at constant V/nD must be interpreted as an increase of power input which yields a disproportionately small return in the form of thrust-power output. Since these models have three blades, the corresponding blade power loading C_p/B is approximately 0.07. This value must not be considered applicable to blades of all plan forms but should be correlated with the activity factor which, in the case of those models, has the relatively large value of 92.4.

The question now arises: How is inefficient operation at reduced values of V/nD to be avoided if, for example, use of the largest diameter compatible with tip speed limitations fails to eliminate the overloading of a propeller of

the selected type? Three alternative methods of escaping from this dilemma suggest themselves:

(a) Adopt a smaller drive gear ratio and an appropriately larger propeller diameter.

(b) Increase the number of blades of the originally selected size and form.

(c) Replace the originally selected blades with an equal number of wider ones.

When a suitable gear ratio is available, method (a) offers a satisfactory solution of the difficulty if the enlarged diameter can be accommodated. The desired result is obtained by reducing C_p which causes the point representing the original operating conditions to be moved from a position close to or behind the crest line (figs. E, 45, and 46) to one well forward of it. The resulting improvement of low speed efficiency in a specific case (Model $P_{C2}(3)$ has been chosen to permit subsequent examination of solidity effects) may be seen in the curves for $C_p = 0.4$ and 0.3 in figure 44. Since C_p varies with $1/D^2$ when power input and tip speed are fixed, such a reduction of C_p (0.4 to 0.3) would require a 15.5 percent increase of diameter. However, at $V/nD = 1.0$, the efficiency would rise from 0.403 to 0.532, a gain of 32 percent.

The alternative method (b) whereby the reduction of C_p/B is obtained through variation of B rather than C_p may now be examined. In this case, improvement is effected by modification of the propeller characteristics which correspond to given values of V/nD and C_p. The origin and character of such modifications may be readily visualized by consideration of figure E.

The effect of increasing the number of blades is substantially equivalent to displacing the thrust-power model through equal distances* in the positive directions of the C_p and ηC_p axes - that is, parallel to a 45° line in the $C_p, \eta C_p$ plane. The fact that η/η_i, rather than η itself,

*The displacements which correspond to the change from three to four blades are equal to the distances between the 0.3 and 0.4 divisions of the scales.

is fixed by blade loading (fig. 43) would require minor distortions of the model to accompany such displacements in the complete physical analogy, but for moderate changes of solidity these are practically negligible when $V/nD > 1.0 > C_p$.

Thus interpreted, the effect of increasing the number of blades is to displace the model while the horizontal coordinates $(V/nD, C_p)$ of the point which represents the operating conditions remain fixed. As the ordinate of the point (ηC_p) is that of the model's surface, it will increase as the displacement forces the representative point off the flat crest onto the steep forward slope. It will be seen that the relative motion of the point with respect to the model is, in this simplified analogy, identical with that for case (a).

Figure 44 shows that with $V/nD = 1.0$ and $C_p = 0.4$, the efficiency of Model P_{C2} is increased from 0.403 to 0.522 by the addition of a fourth blade; the gain is 29.5 percent. It is believed that a 33-percent increase of blade width - method (c) - would produce an almost identical improvement under the same conditions.

The practically negligible difference between the results of increasing diameter and solidity are particularly interesting because the latter is advantageous from the standpoint of weight. If propeller weights vary with D^3, B, and blade width, the weights of the propellers required to reduce the blade loading in the ratio of 3:4 will be $(1.155)^3 W_o = 1.54 W_o$ for case (a) and $1.33 W_o$ for cases (b) and (c). It thus appears that despite the advantages heretofore ascribed to large diameters, it may prove desirable - at least under some conditions - to suppress overloading by increasing solidity rather than diameter.

It is hoped that the foregoing discussion may lead to a more general recognition and better understanding of the phenomena associated with overloading and thus enable clearer analysis of individual propeller selection problems. The hazards of inadequacy will be multiplied as engine capacities and ceilings increase. The utilization of power coefficients as great as 0.6 is now in immediate prospect, and it appears likely that this maximum may soon be doubled if not tripled. With this outlook, it behooves the designers of all high-powered aircraft to consider carefully

the case of the well-known bomber the full load ceiling of which was very substantially augmented by the simple expedient of increasing the width of its propeller blades.

TABLE I

Model U36 Three Blades $\beta_{0.75R} = 12°$

Test No. 123				Test No. 124			
V/nD	C_P	C_T	η	V/nD	C_P	C_T	η
0.614	0.0163	0.0109	0.411	0.593	0.0189	0.0159	0.499
.573	.0214	.0213	.573	.552	.0243	.0266	.604
.534	.0261	.0316	.647	.512	.0283	.0362	.655
.492	.0303	.0414	.672	.471	.0321	.0458	.672
.449	.0339	.0512	.678	.434	.0350	.0536	.665
.408	.0365	.0592	.662	.394	.0378	.0622	.648
.370	.0385	.0670	.644	.357	.0396	.0701	.632
.326	.0405	.0754	.607	.306	.0416	.0790	.581
.285	.0416	.0818	.560	.268	.0425	.0843	.532
.250	.0422	.0873	.517	.219	.0433	.0919	.465
.208	.0429	.0930	.451				

TABLE II

Model U36 Three Blades $\beta_{0.75R} = 24°$

Test No. 127				Test No. 128			
V/nD	C_P	C_T	η	V/nD	C_P	C_T	η
1.175	0.0163	0.0052	0.375	1.149	0.0242	0.0127	0.603
1.121	.0307	.0192	.701	1.093	.0391	.0278	.777
1.071	.0425	.0323	.814	1.047	.0507	.0402	.830
1.018	.0568	.0473	.848	.993	.0618	.0526	.845
.969	.0679	.0589	.841	.943	.0728	.0658	.852
.915	.0774	.0713	.843	.890	.0823	.0782	.846
.861	.0866	.0841	.836	.839	.0895	.0886	.831
.813	.0922	.0931	.821	.788	.0946	.0975	.812
.764	.0961	.0999	.794	.737	.0984	.1054	.789
.711	.0998	.1090	.777	.686	.1014	.1129	.764
.661	.1029	.1168	.750	.631	.1044	.1211	.732
.609	.1047	.1230	.715	.585	.1055	.1261	.699
.559	.1065	.1288	.676	.533	.1079	.1319	.652
.507	.1090	.1341	.624	.479	.1121	.1371	.586
.456	.1145	.1370	.546	.434	.1182	.1378	.506
.404	.1235	.1381	.452	.381	.1274	.1408	.421
.353	.1286	.1422	.390	.325	.1325	.1440	.353
.304	.1347	.1453	.328	.280	.1367	.1470	.301
.251	.1400	.1490	.267				

TABLE III

Model U36 Three Blades $\beta_{0.75R} = 36°$

Test No. 131				Test No. 132			
V/nD	C_P	C_T	η	V/nD	C_P	C_T	η
1.842	0.0388	0.0114	0.541	1.806	0.0498	0.0188	0.682
1.778	.0640	.0264	.705	1.731	.0790	.0374	.819
1.695	.0913	.0453	.841	1.663	.1050	.0542	.858
1.621	.1185	.0632	.865	1.586	.1315	.0726	.876
1.551	.1408	.0794	.874	1.519	.1500	.0861	.872
1.477	.1609	.0952	.874	1.445	.1677	.1010	.870
1.397	.1740	.1076	.864	1.367	.1787	.1121	.858
1.323	.1844	.1184	.849	1.299	.1891	.1229	.844
1.248	.1936	.1287	.830	1.218	.1978	.1333	.821
1.177	.2014	.1386	.810	1.145	.2051	.1427	.797
1.103	.2085	.1467	.776	1.071	.2123	.1502	.758
1.026	.2169	.1541	.729	1.005	.2223	.1562	.706
.954	.2270	.1553	.653	.920	.2336	.1549	.610
.880	.2350	.1546	.579	.846	.2385	.1544	.548
.805	.2420	.1555	.517	.773	.2495	.1561	.484
.736	.2499	.1568	.462	.700	.2546	.1577	.434
.659	.2582	.1598	.408	.621	.2610	.1614	.384
.589	.2648	.1630	.363	.557	.2660	.1639	.343
.510	.2713	.1666	.313	.473	.2727	.1676	.291
.447	.2755	.1693	.275	.401	.2798	.1716	.246
.370	.2818	.1729	.227				

TABLE IV

Model U36 Three Blades $\beta_{0.75R} = 48°$

Test No. 135				Test No. 136			
V/nD	C_P	C_T	η	V/nD	C_P	C_T	η
2.617	0.1904	0.0571	0.785	2.583	0.2091	0.0653	0.807
2.529	.2236	.0727	.822	2.491	.2448	.0820	.834
2.425	.2659	.0925	.844	2.380	.2864	.1026	.853
2.330	.2985	.1102	.860	2.284	.3072	.1168	.868
2.228	.3161	.1217	.858	2.179	.3261	.1289	.861
2.120	.3333	.1338	.851	2.075	.3423	.1399	.848
2.025	.3493	.1460	.846	1.966	.3564	.1515	.836
1.925	.3614	.1560	.831	1.870	.3690	.1616	.819
1.817	.3741	.1653	.803	1.773	.3768	.1682	.791
1.712	.3835	.1716	.766	1.666	.3886	.1732	.743
1.615	.3928	.1718	.706	1.564	.3911	.1669	.667
1.508	.3878	.1625	.632	1.469	.3861	.1601	.609
1.405	.3813	.1569	.578	1.361	.3810	.1560	.557
1.304	.3814	.1536	.525	1.258	.3812	.1504	.496
1.209	.3844	.1498	.471	1.160	.3889	.1500	.447
1.104	.3926	.1519	.427	1.062	.3963	.1520	.407
1.005	.4027	.1551	.387	.956	.4067	.1564	.368
.894	.4101	.1573	.343	.860	.4175	.1605	.331
.820	.4233	.1630	.316	.754	.4299	.1665	.292
.711	.4322	.1675	.276	.661	.4385	.1691	.255
.601	.4379	.1699	.233	.550	.4438	.1721	.213
.506	.4430	.1727	.197				

TABLE V

Model U36 Three Blades $\beta_{0.75R} = 60°$

Test No. 139				Test No. 140			
V/nD	C_P	C_T	η	V/nD	C_P	C_T	η
3.626	0.6564	0.1420	0.784	3.790	0.6142	0.1234	0.761
3.505	.6774	.1543	.798	3.706	.6375	.1333	.775
3.344	.6902	.1648	.798	3.571	.6734	.1502	.797
3.211	.6985	.1736	.798	3.402	.6876	.1604	.794
3.050	.7089	.1850	.796	3.267	.6972	.1710	.801
2.907	.7166	.1939	.787	3.122	.7026	.1798	.799
2.750	.7098	.1944	.753	2.964	.7096	.1903	.795
2.607	.7048	.1942	.718	2.839	.7117	.1949	.777
2.462	.6857	.1839	.660	2.684	.7099	.1984	.750
2.330	.6369	.1589	.581	2.528	.6954	.1908	.694
2.170	.5791	.1274	.477	2.396	.6646	.1739	.627
2.010	.5499	.1117	.408	2.241	.5983	.1387	.520
1.873	.5420	.1081	.374	2.096	.5643	.1182	.439
1.731	.5420	.1083	.346	1.952	.5457	.1104	.395
1.580	.5596	.1131	.319	1.800	.5410	.1083	.360
1.450	.5738	.1186	.300	1.662	.5494	.1106	.335
1.312	.5851	.1223	.274	1.516	.5653	.1156	.310
1.160	.5908	.1267	.249	1.374	.5809	.1203	.285
1.024	.5950	.1290	.222	1.218	.5900	.1242	.256
.874	.5956	.1354	.199	1.085	.5914	.1267	.232
.717	.5950	.1385	.167	.940	.5936	.1297	.205
				.805	.5978	.1381	.186

TABLE VI

Angles of Attack and Efficiencies for Six Representative Conditions of Operation

	(I) High Speed				(II) Climb			
$C_p = 0.5$	V/nD = 2.85				V/nD = 1.71			
Model	α_{max}	α_{min}	$\Delta\alpha$	η	α_{max}	α_{min}	$\Delta\alpha$	η
U24	20.2	7.4	12.8	0.826	26.6	21.5	5.1	0.474
U36	16.7	8.0	8.7	.835	23.5	23.4	0.1	.463
U48	10.6	8.9	1.7	.839	23.4	16.4	7.0	.511
U60	10.4	3.2	7.2	.829	23.6	8.3	15.3	.526
0.4E	15.4	- 3.0	18.4	.783	27.5	1.2	26.3	.557
0.6E	12.9	3.6	9.3	.819	25.7	8.6	17.1	.550
0.8E	10.8	7.3	3.5	.835	23.6	15.8	7.8	.546
$P_{C2}(3)$	9.6	6.6	3.0	.838	22.6	11.7	10.9	.517
$C_p = 0.2$	V/nD = 1.80				V/nD = 1.08			
U24	11.1	5.2	5.9	0.866	14.0	13.6	0.4	0.792
U36	7.6	6.7	0.9	.873	15.7	11.1	4.6	.788
U48	7.3	1.3	6.0	.873	15.5	4.4	11.1	.788
U60	8.9	- 5.7	14.4	.837	15.1	- 3.3	18.4	.754
0.4E	13.3	-12.4	25.7	.791	17.0	-11.0	28.0	.723
0.6E	11.2	- 5.3	16.5	.829	15.2	- 3.6	18.8	.751
0.8E	9.1	1.9	7.2	.862	14.5	4.3	10.2	.781
$P_{C2}(3)$	8.1	- 2.2	10.3	.862	15.5	0.7	14.8	.781
$C_p = 0.05$	V/nD = 0.90				V/nD = 0.54			
U24	5.5	3.7	1.8	0.843	13.3	4.8	8.5	0.762
U36	7.0	1.2	5.8	.833	14.5	3.1	11.4	.751
U48	6.5	- 5.2	11.7	.811	12.7	2.6	10.1	.745
U60	5.8	-12.7	18.5	.820	10.4	- 4.7	15.1	.762
0.4E	7.2	-19.9	27.1	.773	8.5	-11.8	20.3	.758
0.6E	5.5	-12.4	17.9	.806	8.5	- 4.5	13.0	.762
0.8E	5.0	- 5.3	10.3	.833	10.5	2.8	7.7	.771
$P_{C2}(3)$	6.7	- 8.6	15.3	.825	12.0	- 1.0	13.0	.747

Angles of attack are given in degrees

$\Delta\alpha = \alpha_{max} - \alpha_{min}$

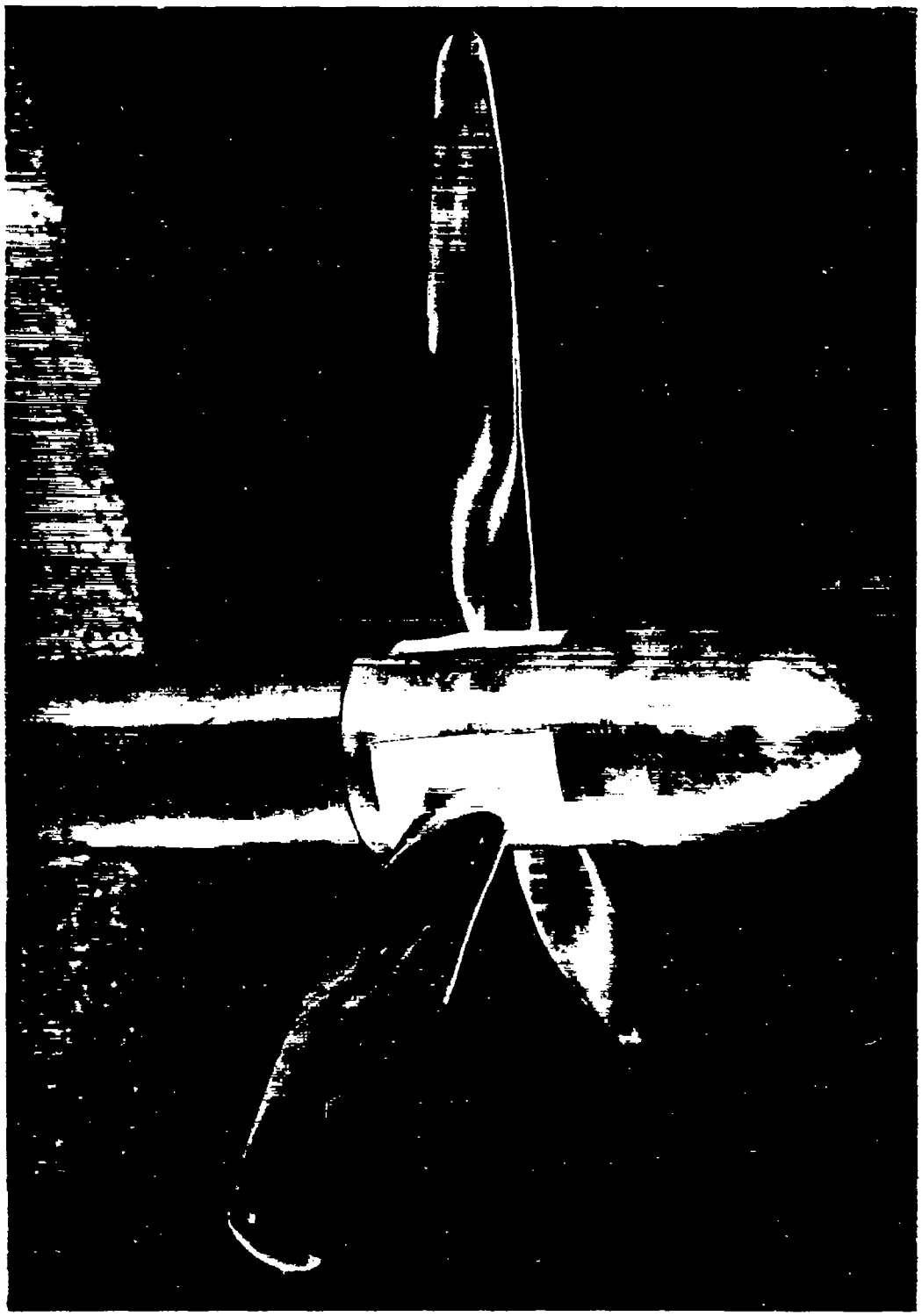

Figure A.- Model on dynamometer.

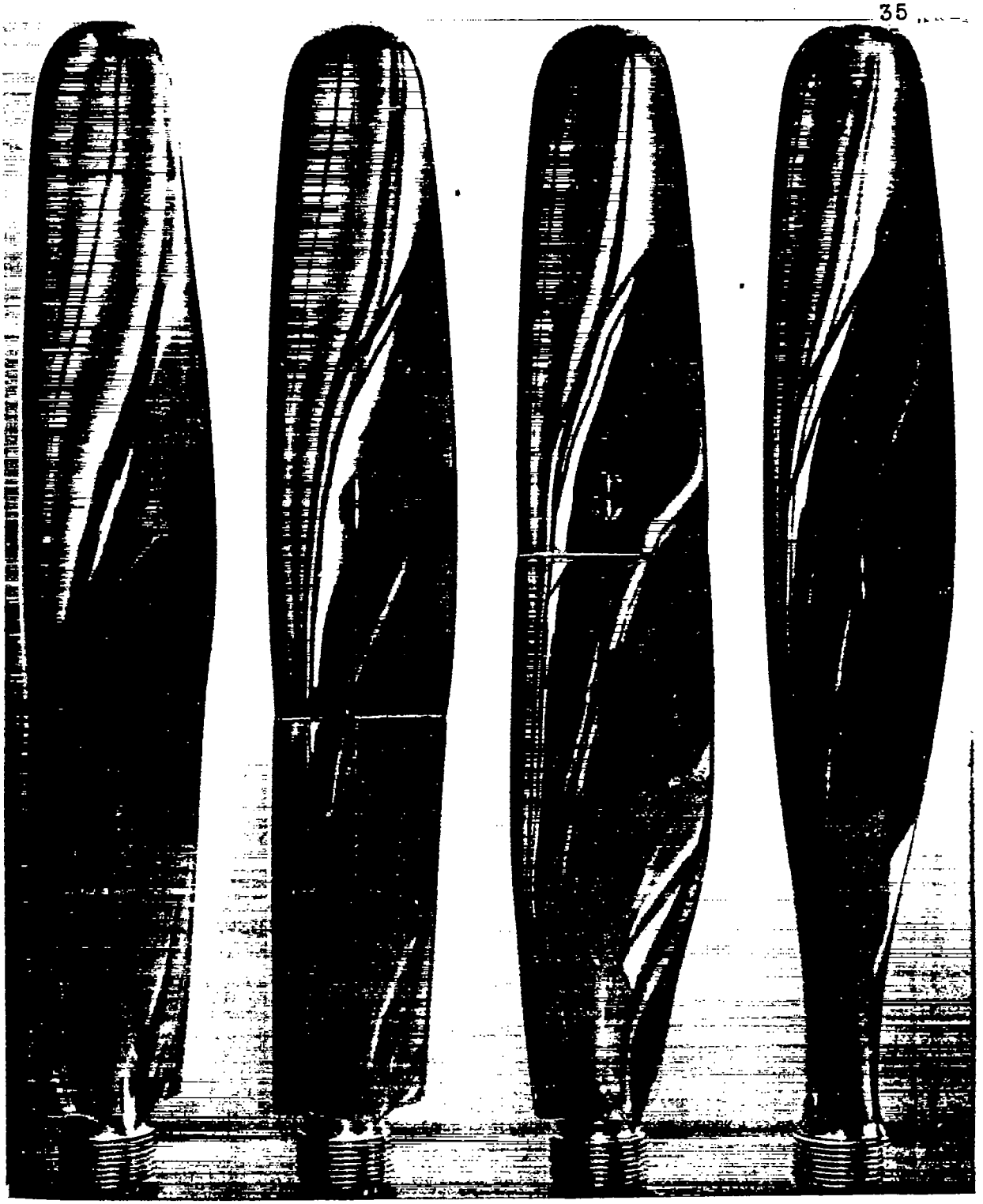

Figure B.- Representative blades - plan view. Left to right: P_{C1}, P_{CS}, P_C, P.

Figure C.- Representative blades - edge view. Left to right: P_{C1}, P_{CS}, P_C, P.

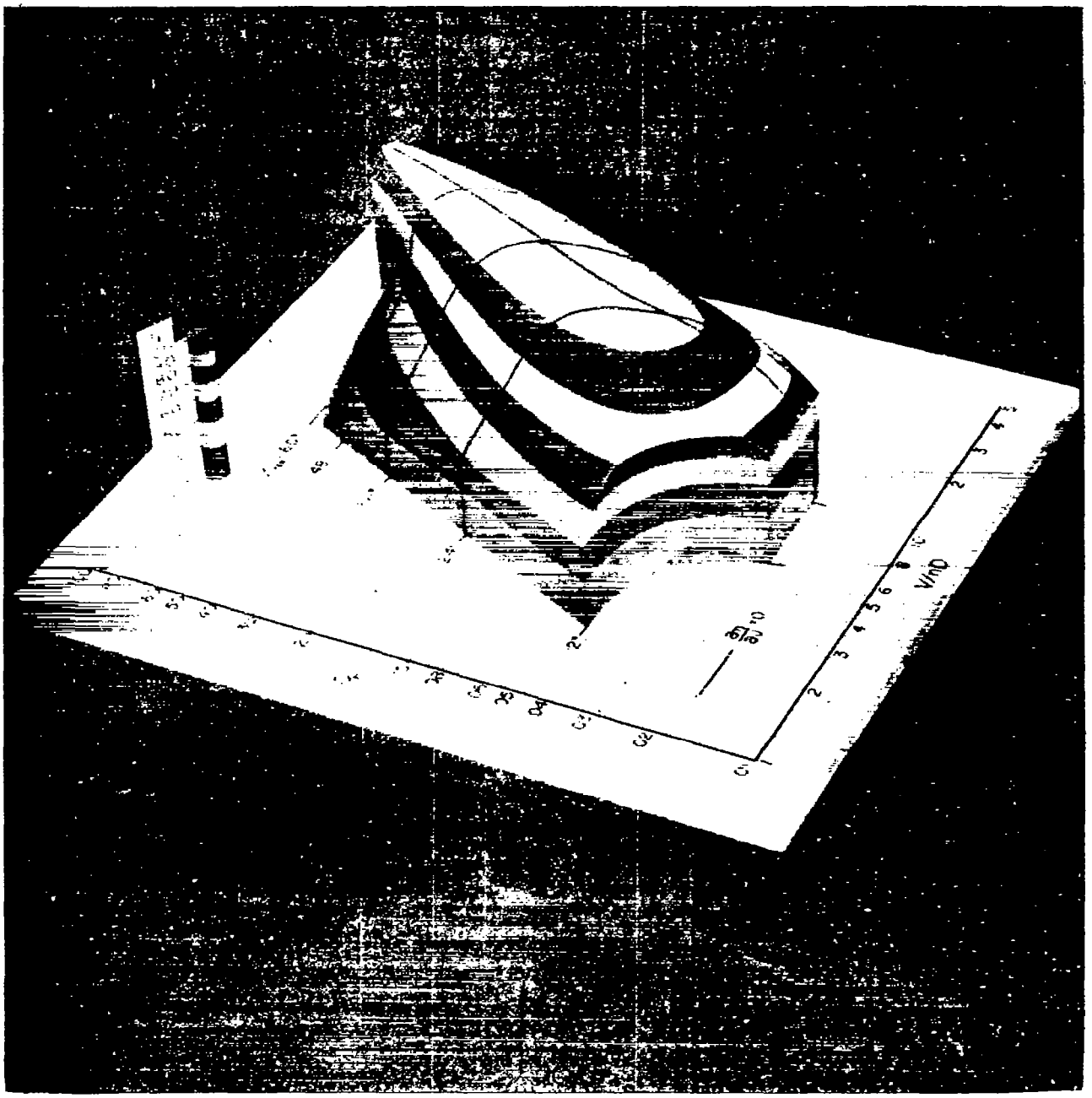

Figure D.- Efficiency model.

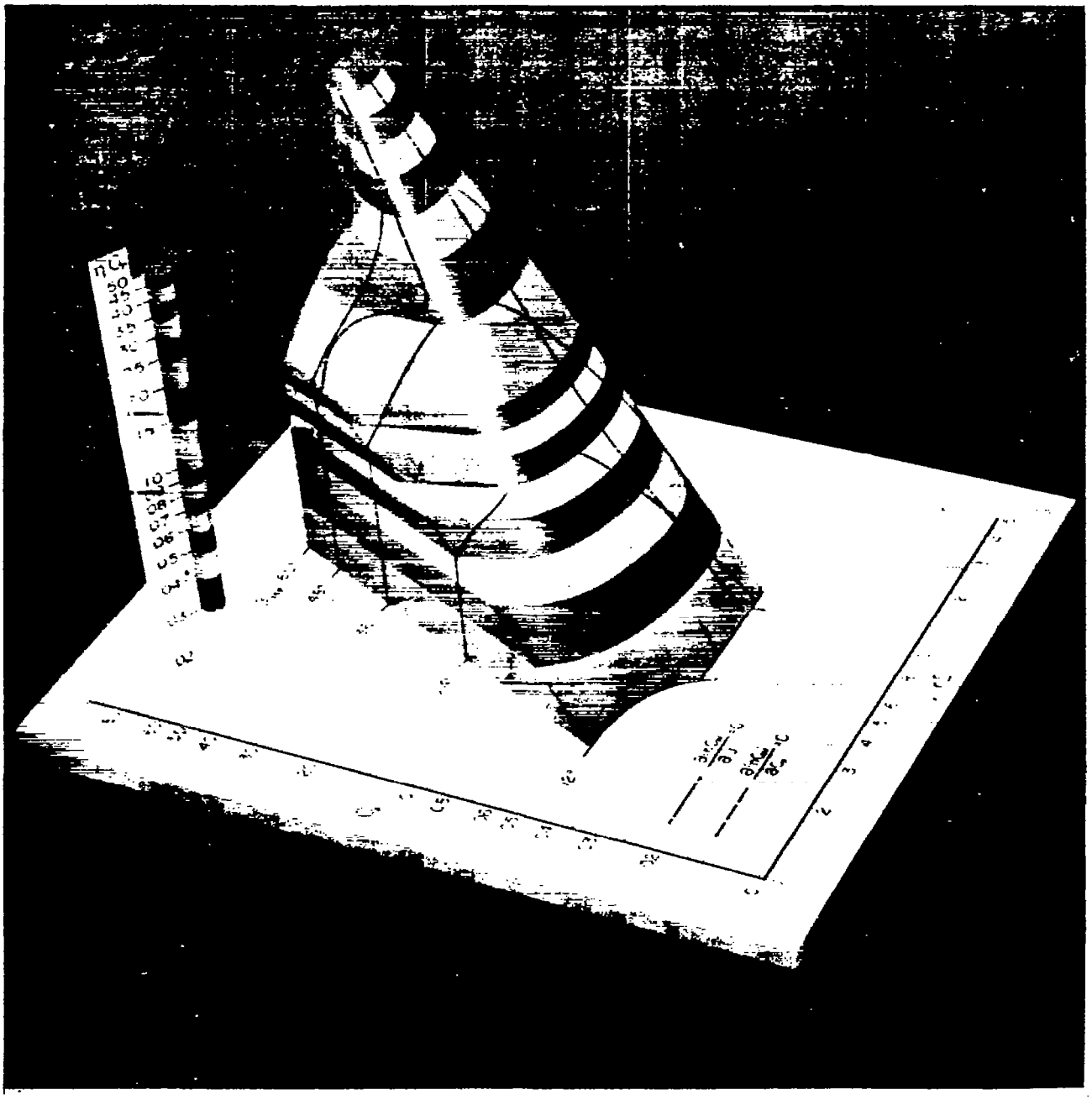

Figure E.- Thrust power model.

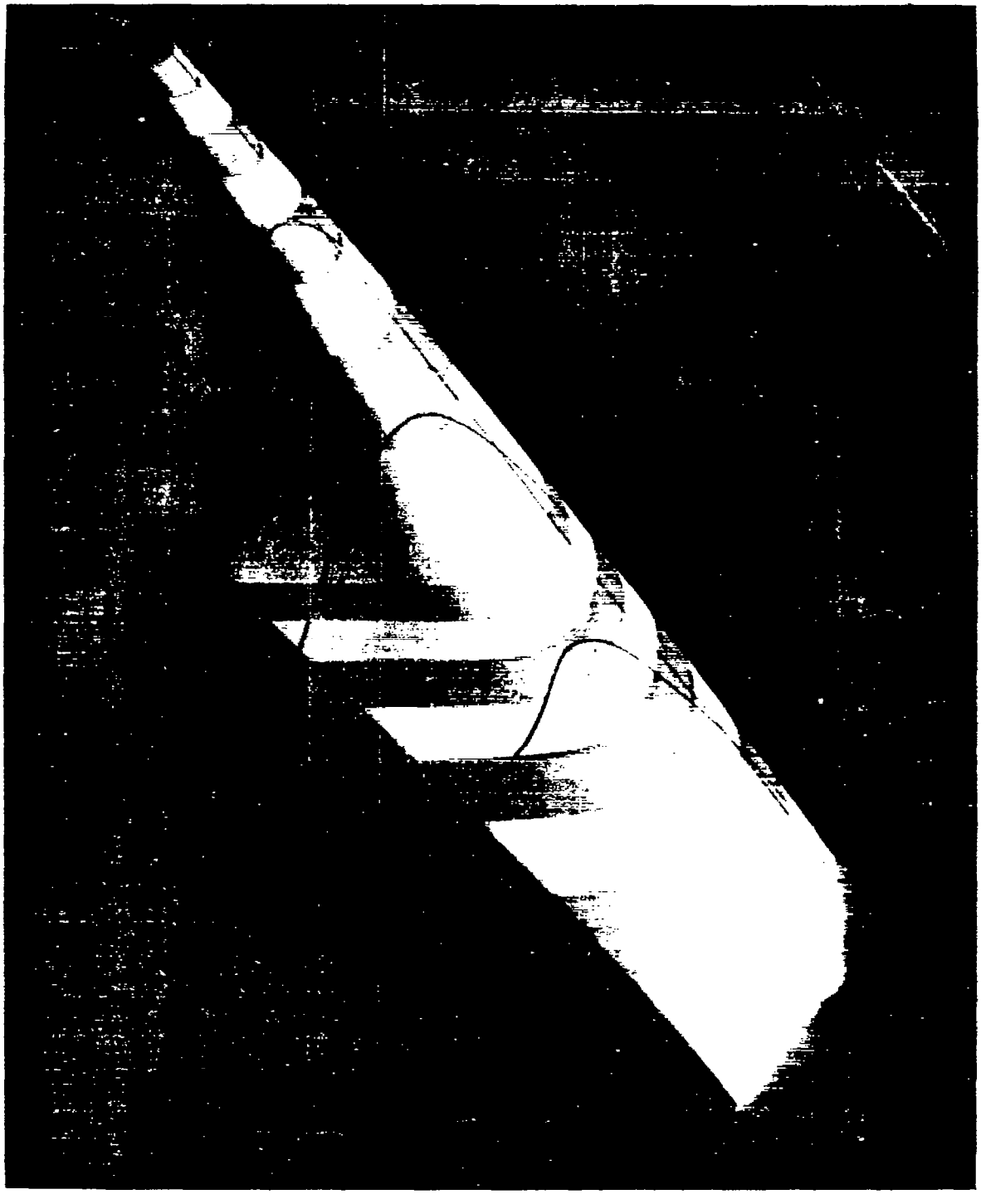

Figure F.- Thrust power model (showing definition of crest by light beam).

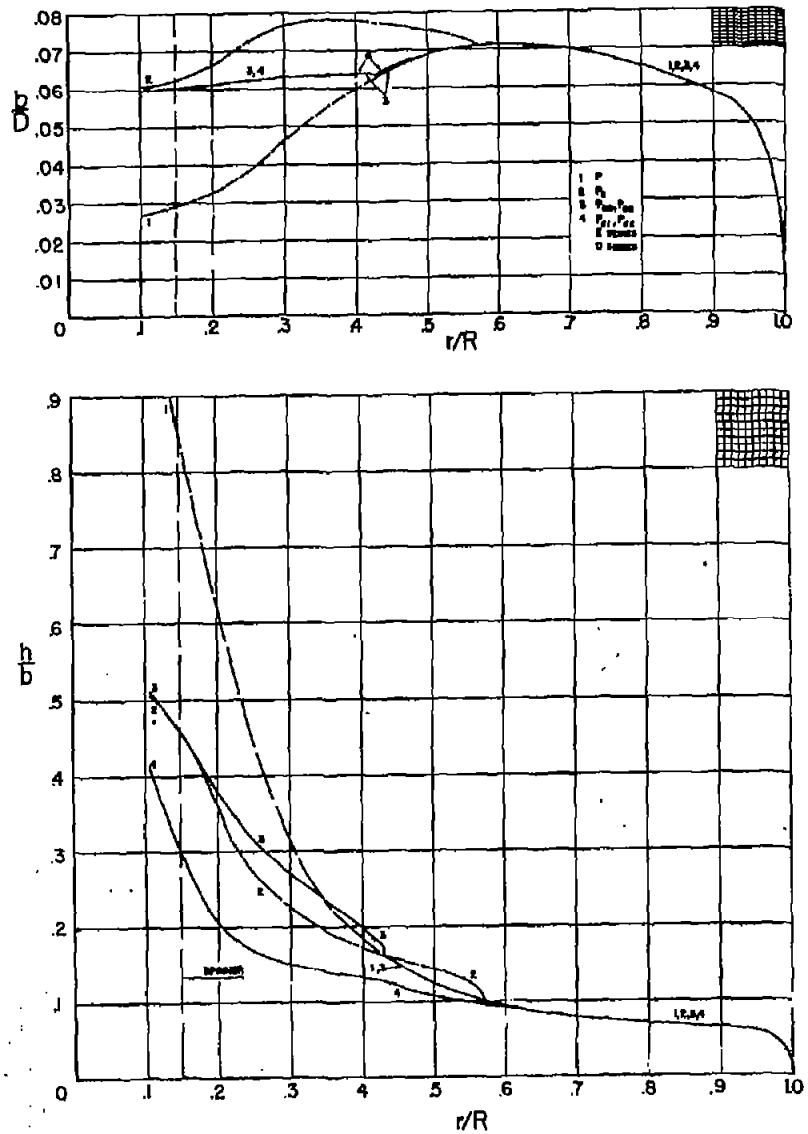

Figure 1.- Blade width and thickness curves.

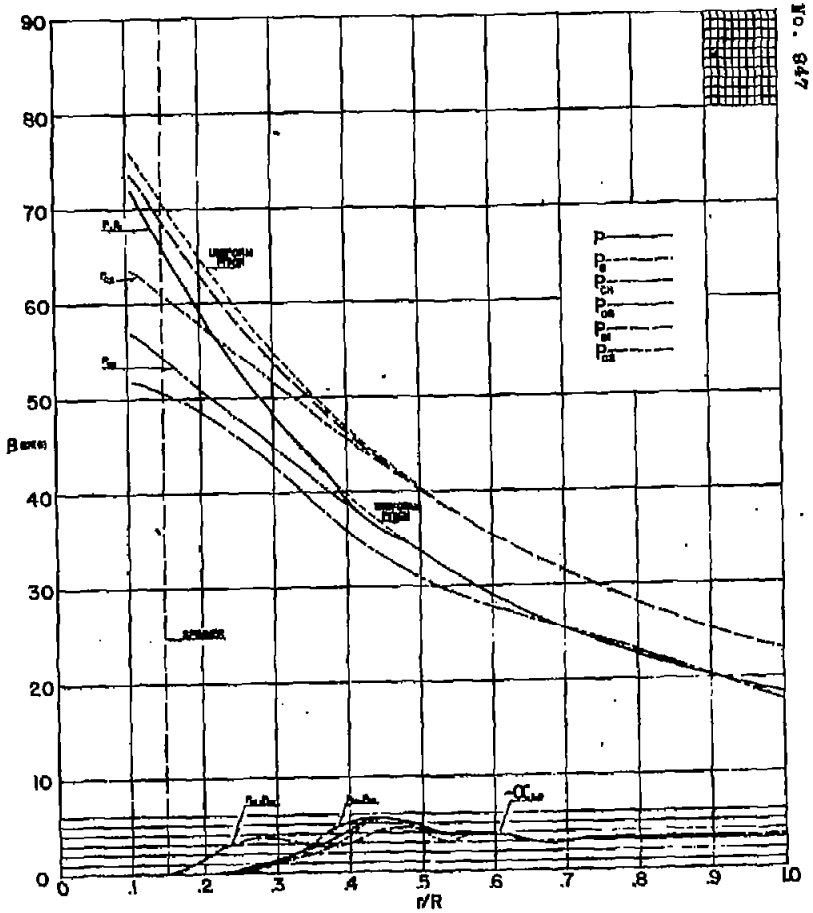

Figure 2.- Design blade angles - P series.

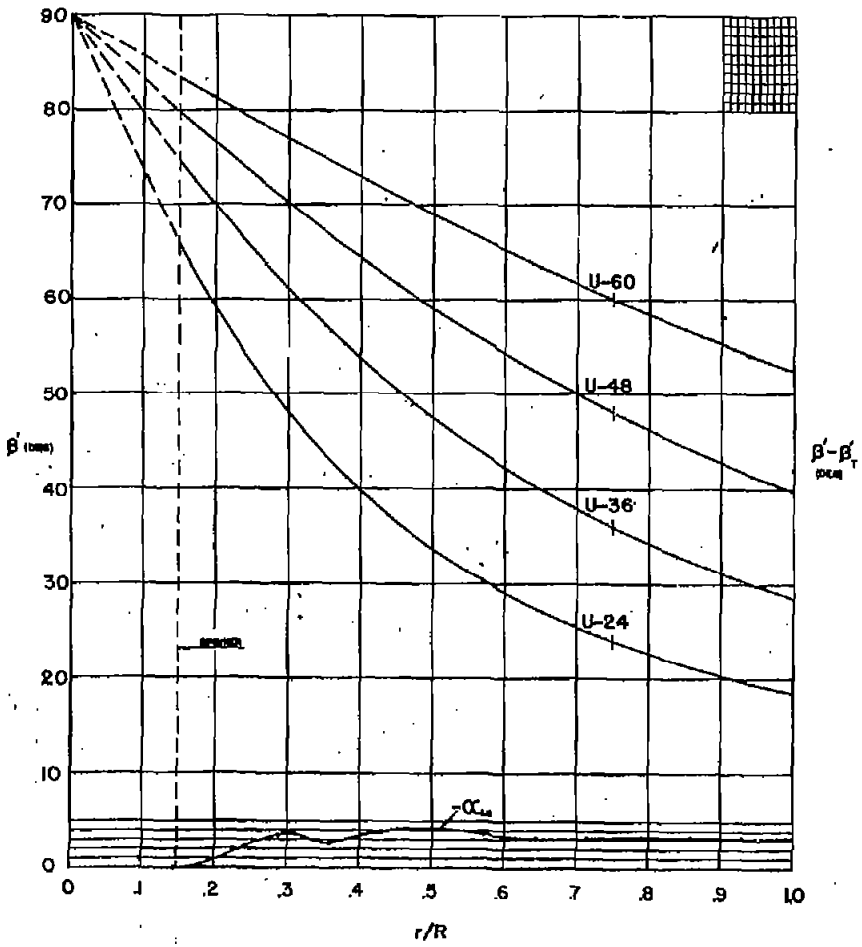

Figure 3.- Design blade angles - U series.

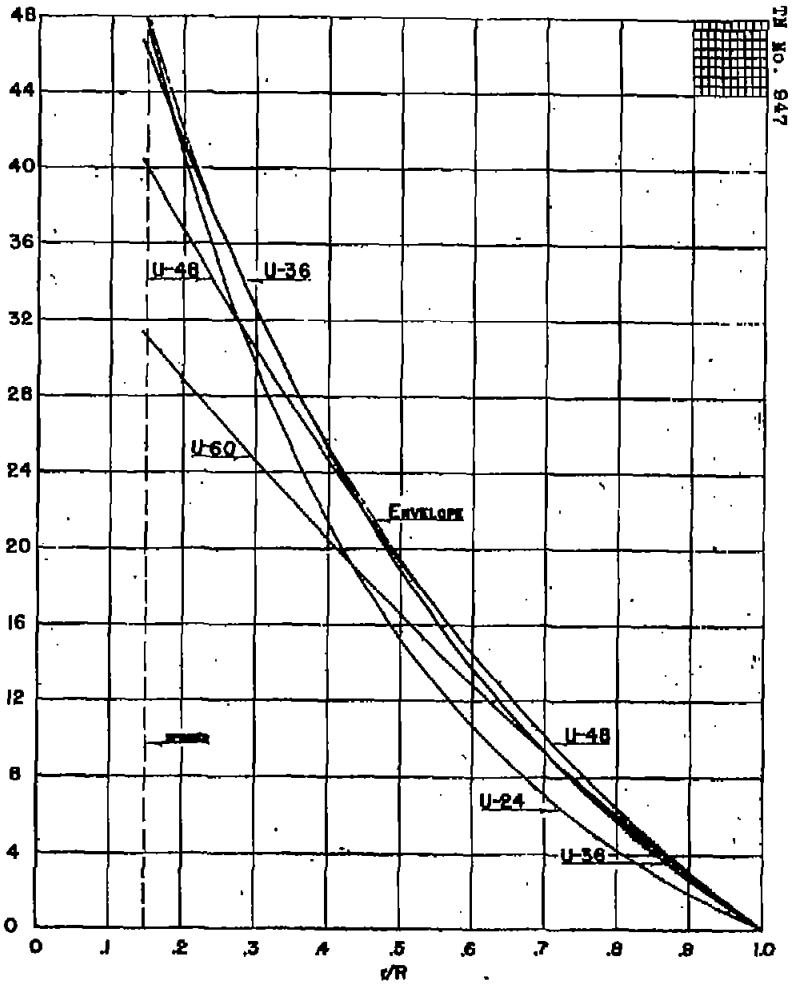

Figure 4.- Blade twist curves - U series.

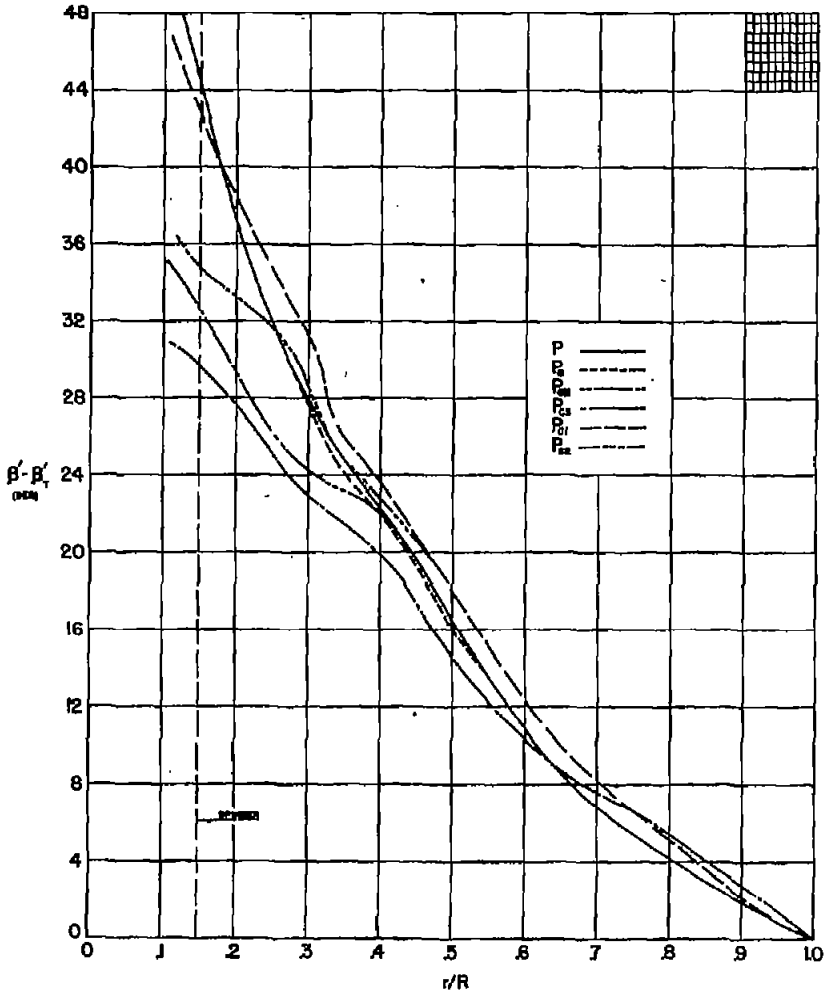

Figure 5.- Blade twist curves - P series.

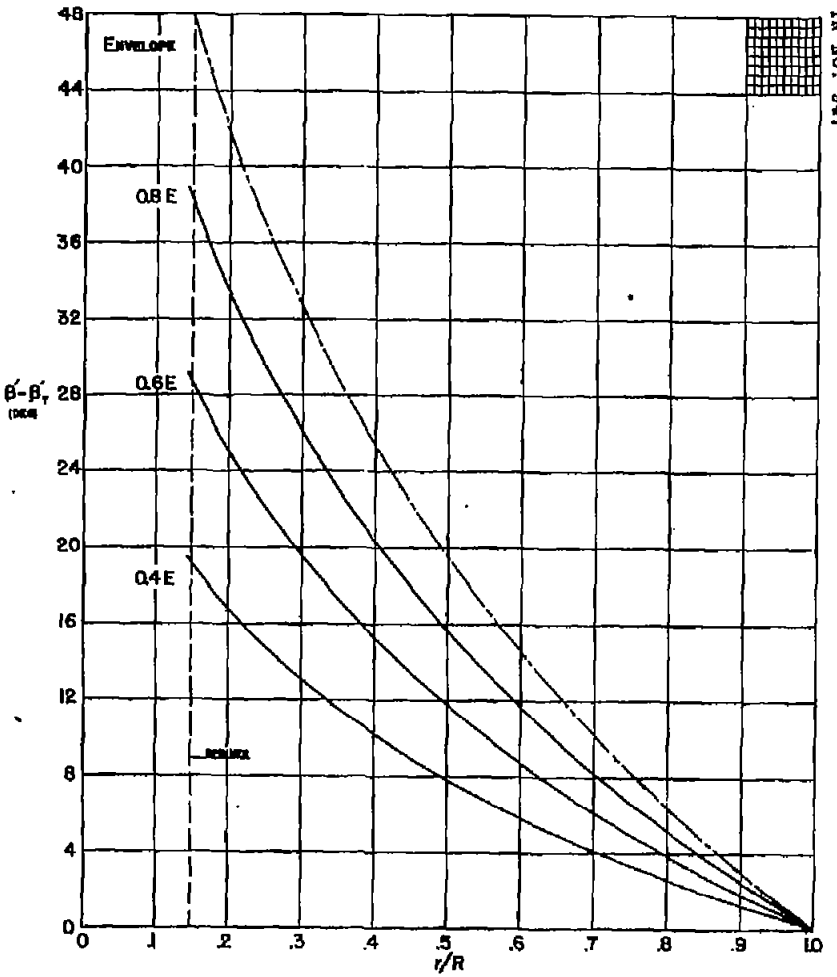

Figure 6.- Blade twist curves - E series.

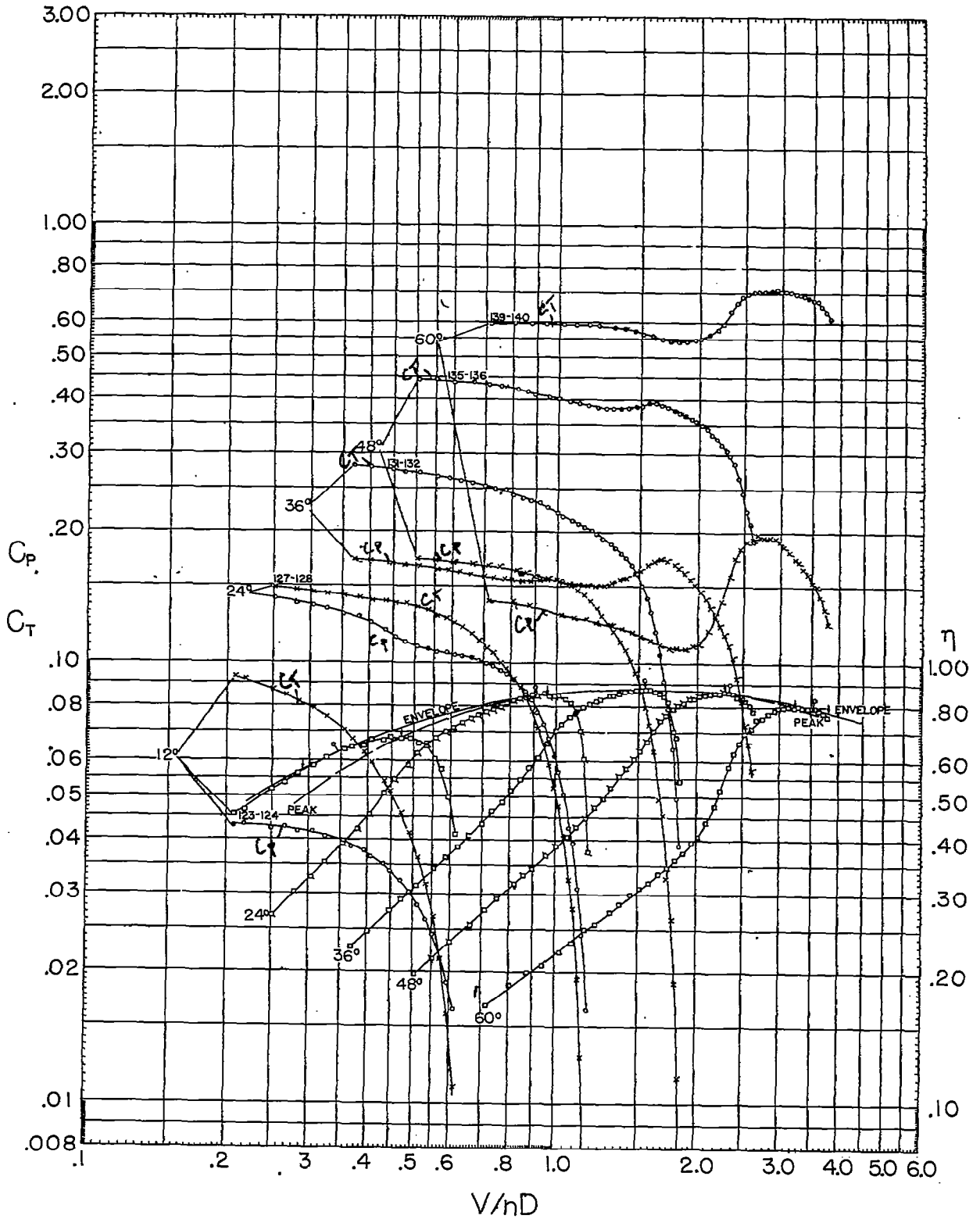

FIGURE 7.- TYPICAL TEST RESULTS-MODEL U36.

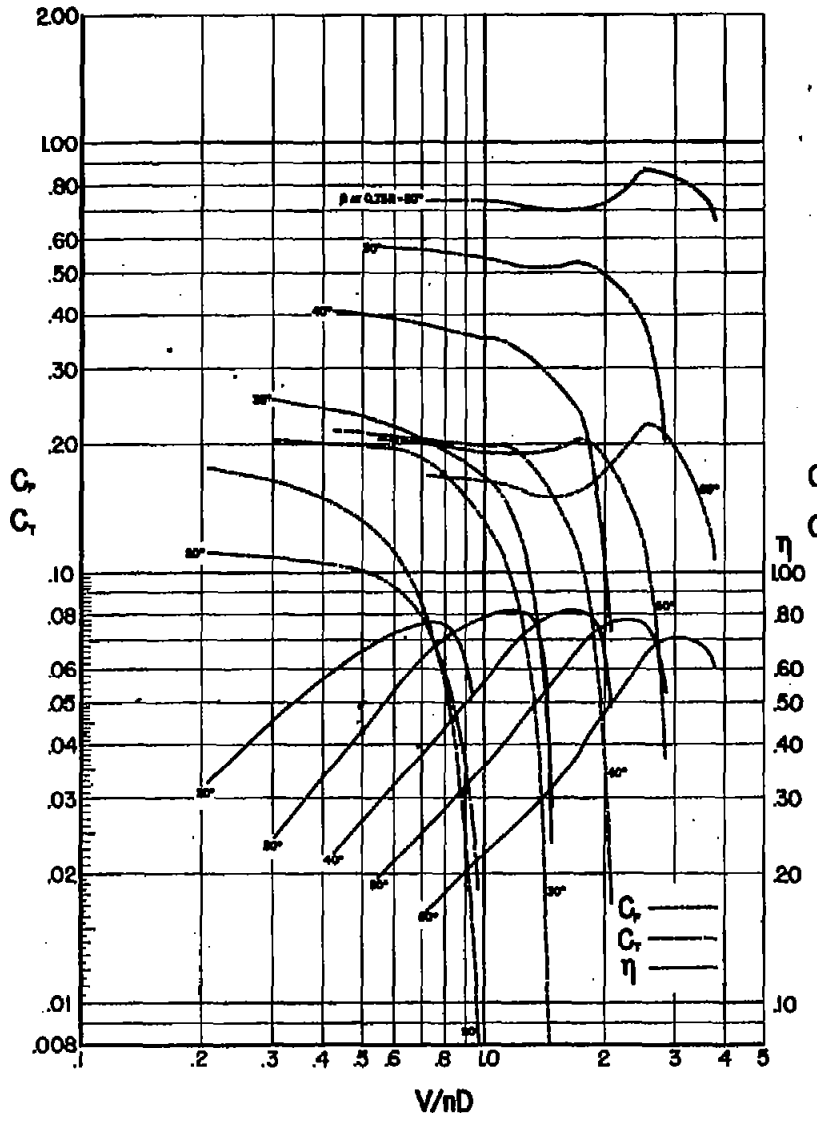

Figure 8.- Characteristics of Model P.

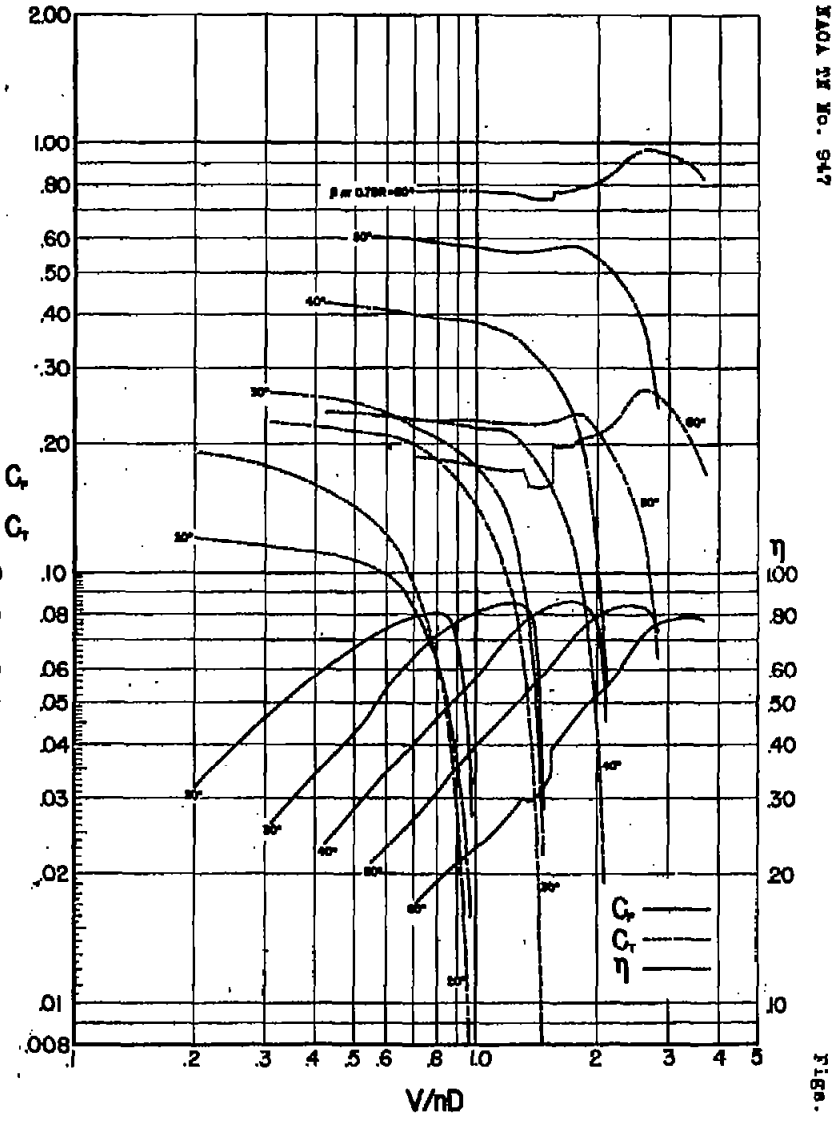

Figure 9.- Characteristics of Model P_0.

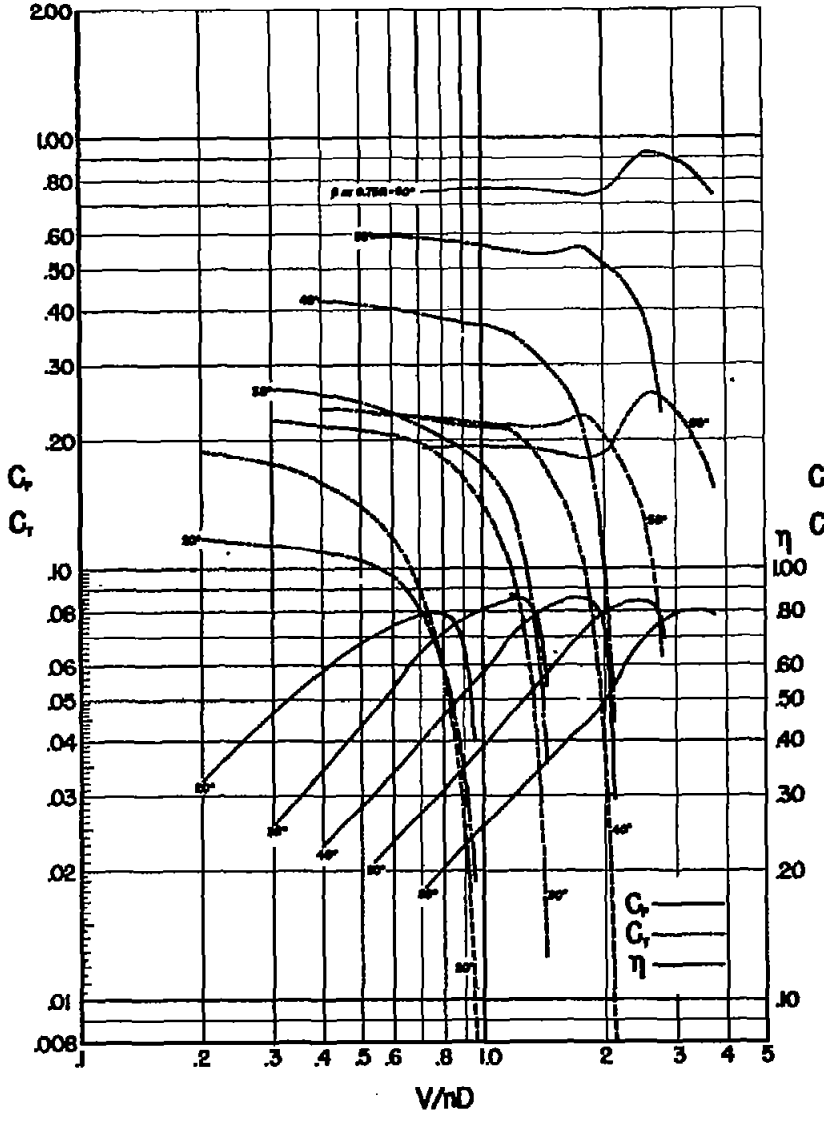

Figure 10.- Characteristics of Model P_{CH}.

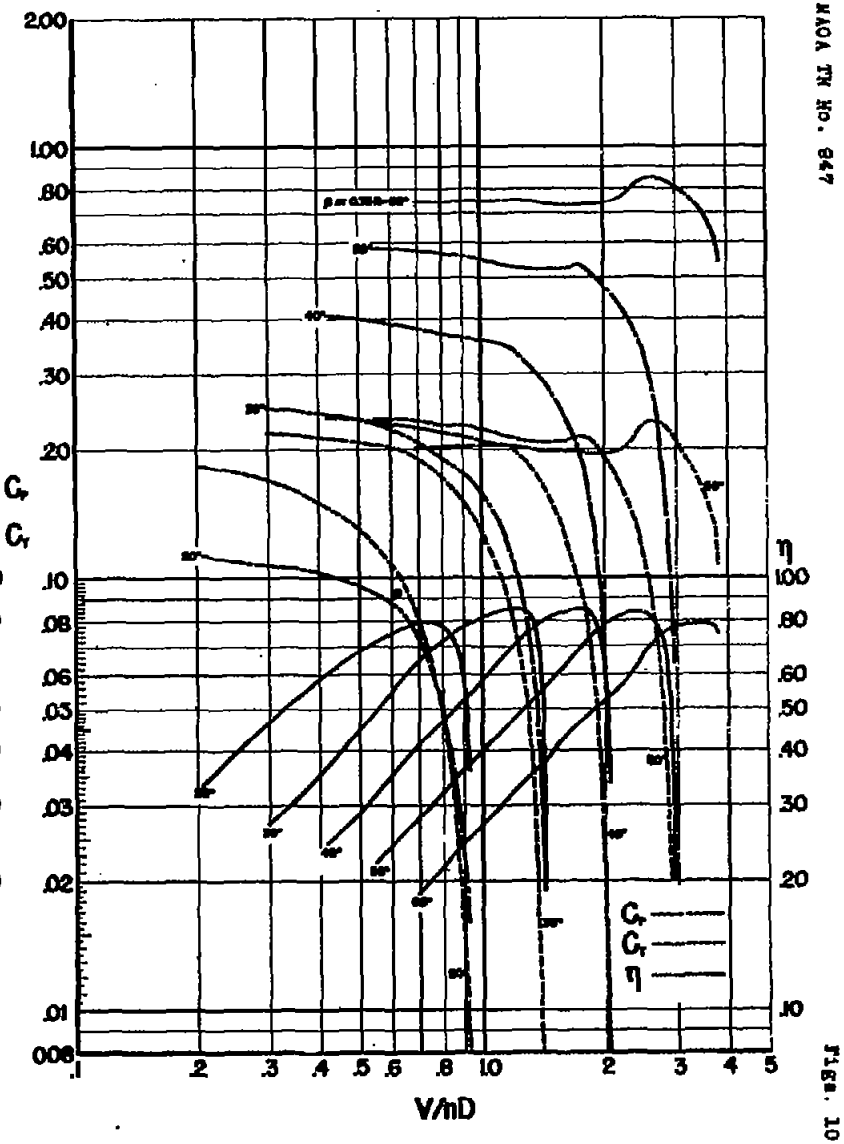

Figure 11.- Characteristics of Model P_{CS}.

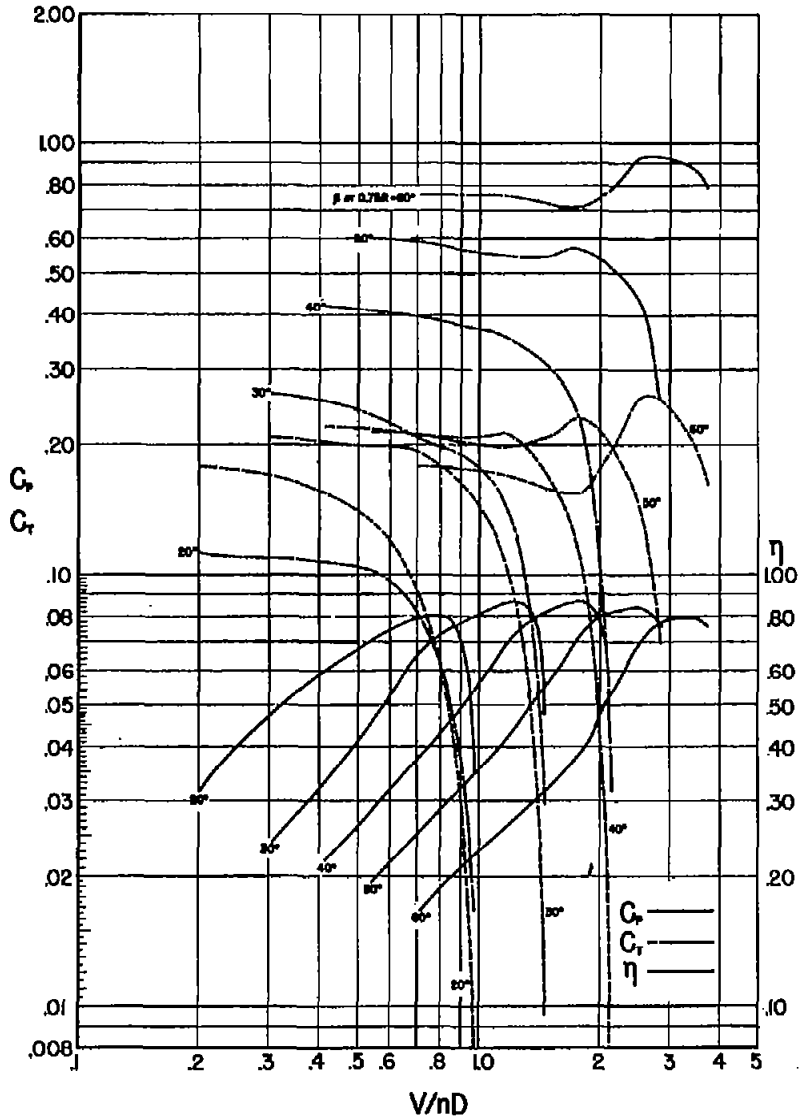

Figure 12.- Characteristics of Model P_{C1}.

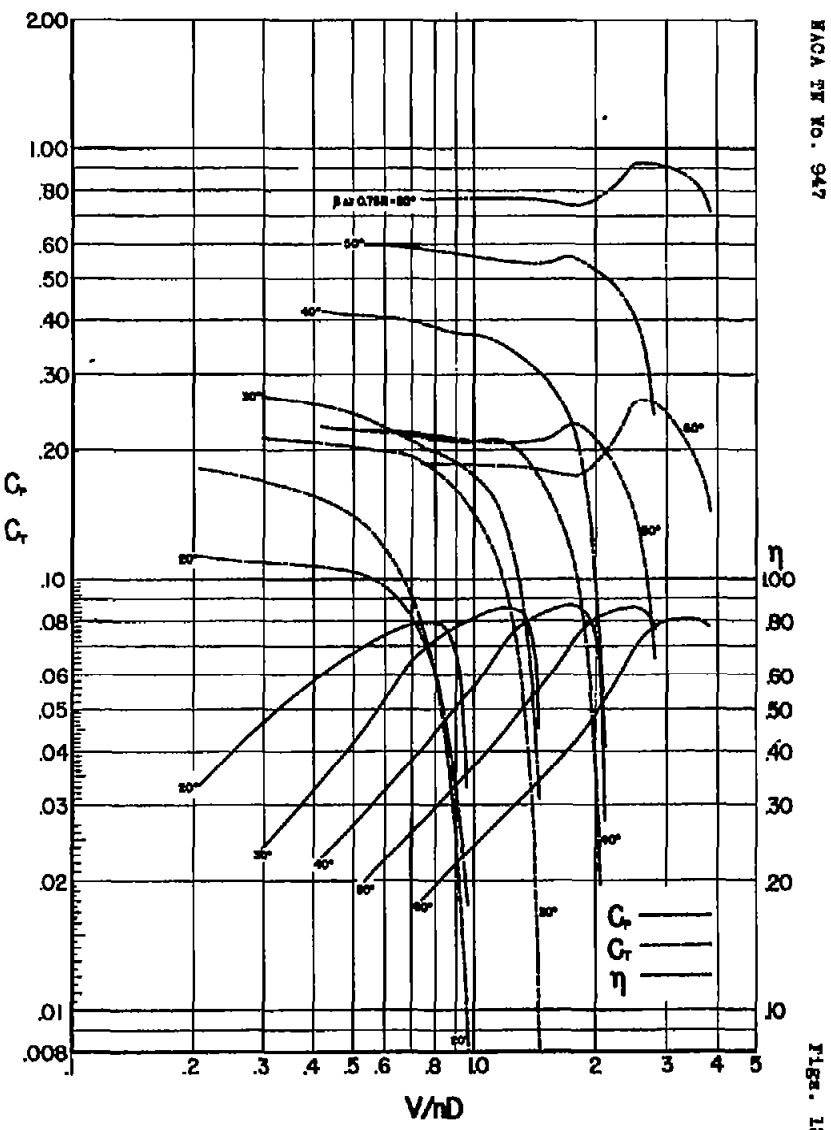

Figure 13.- Characteristics of Model P_{C2}.

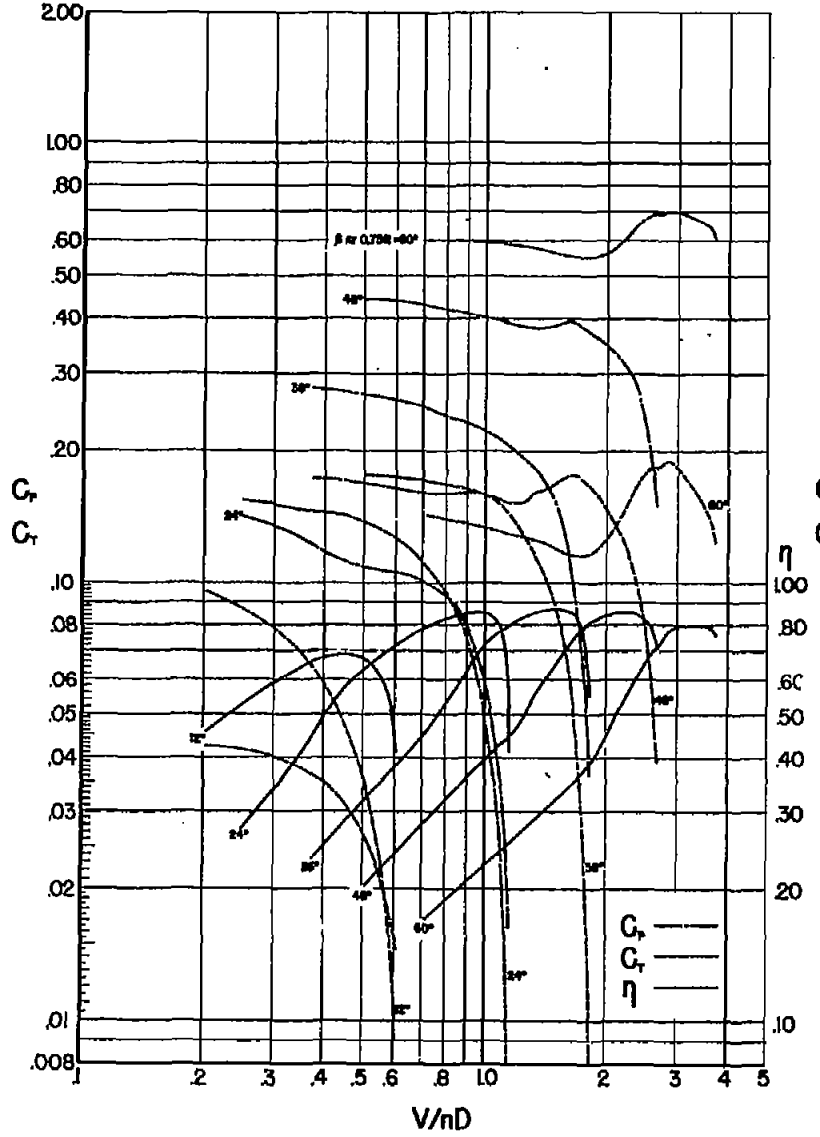

Figure 14.- Characteristics of Model U24.

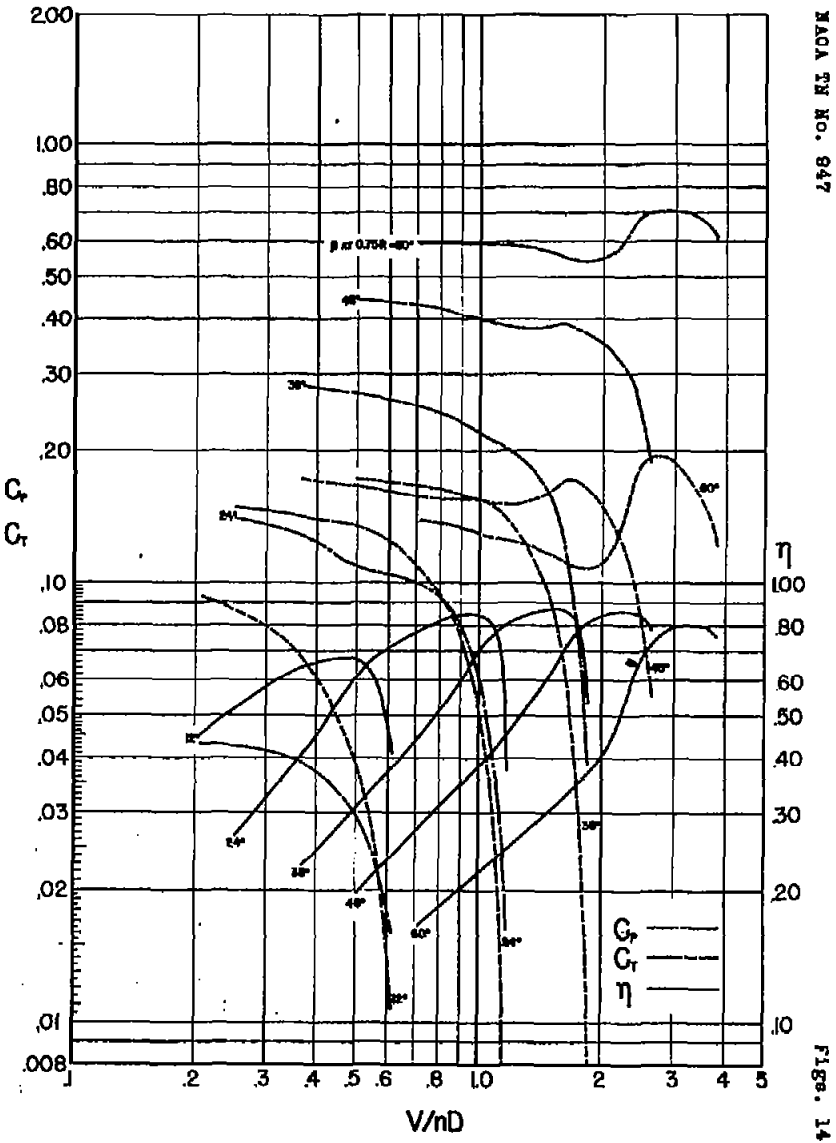

Figure 15.- Characteristics of Model U36.

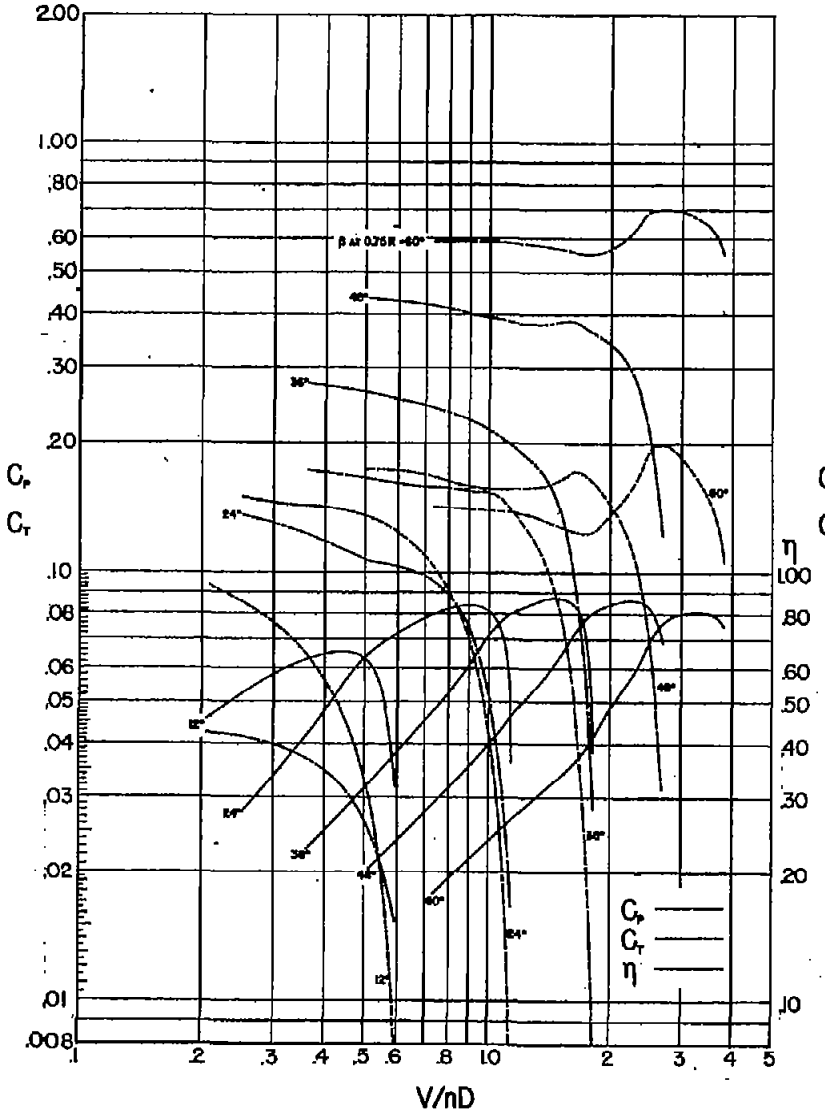

Figure 16.- Characteristics of Model U48.

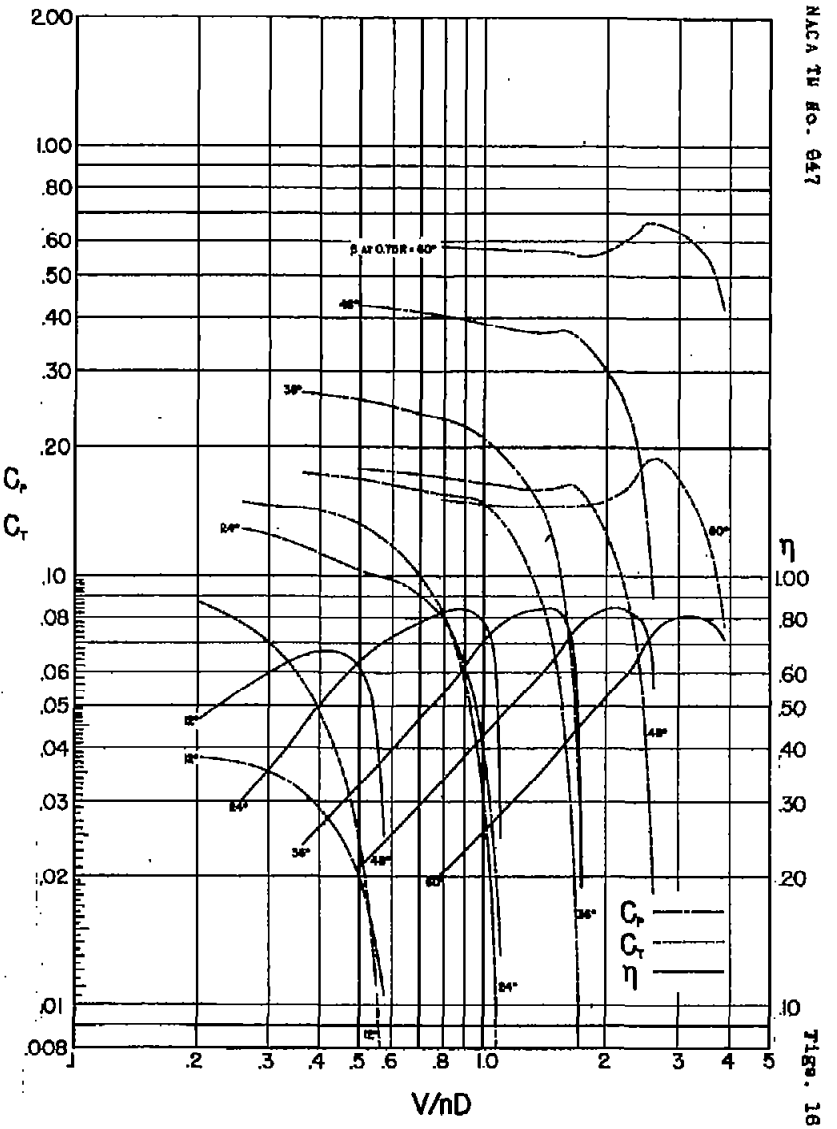

Figure 17.- Characteristics of Model U60.

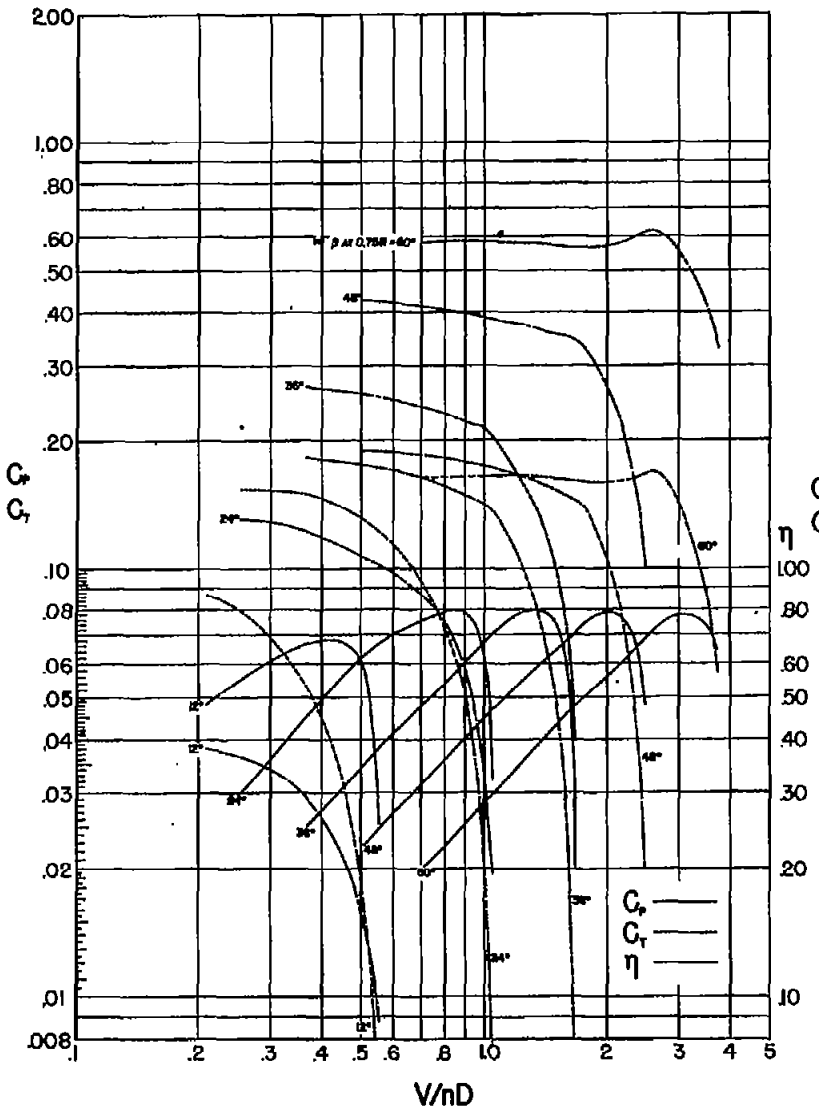

Figure 18.- Characteristics of Model 0.4E.

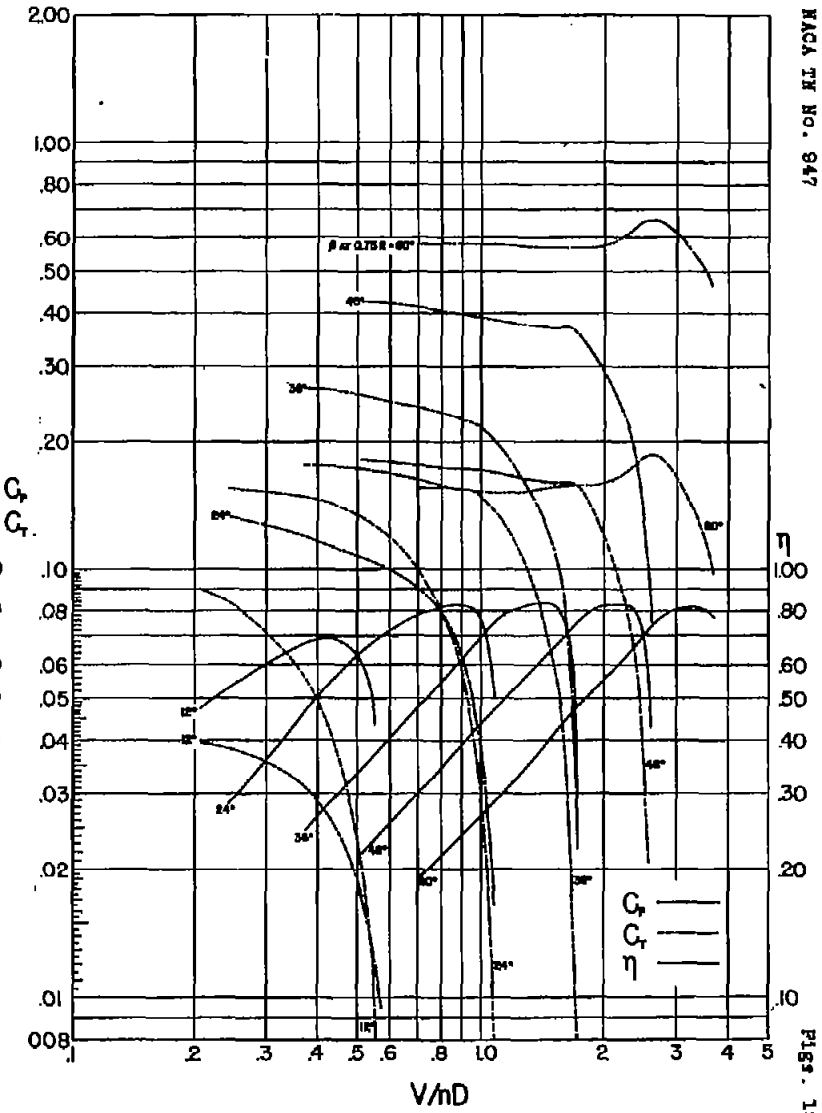

Figure 19.- Characteristics of Model 0.6E.

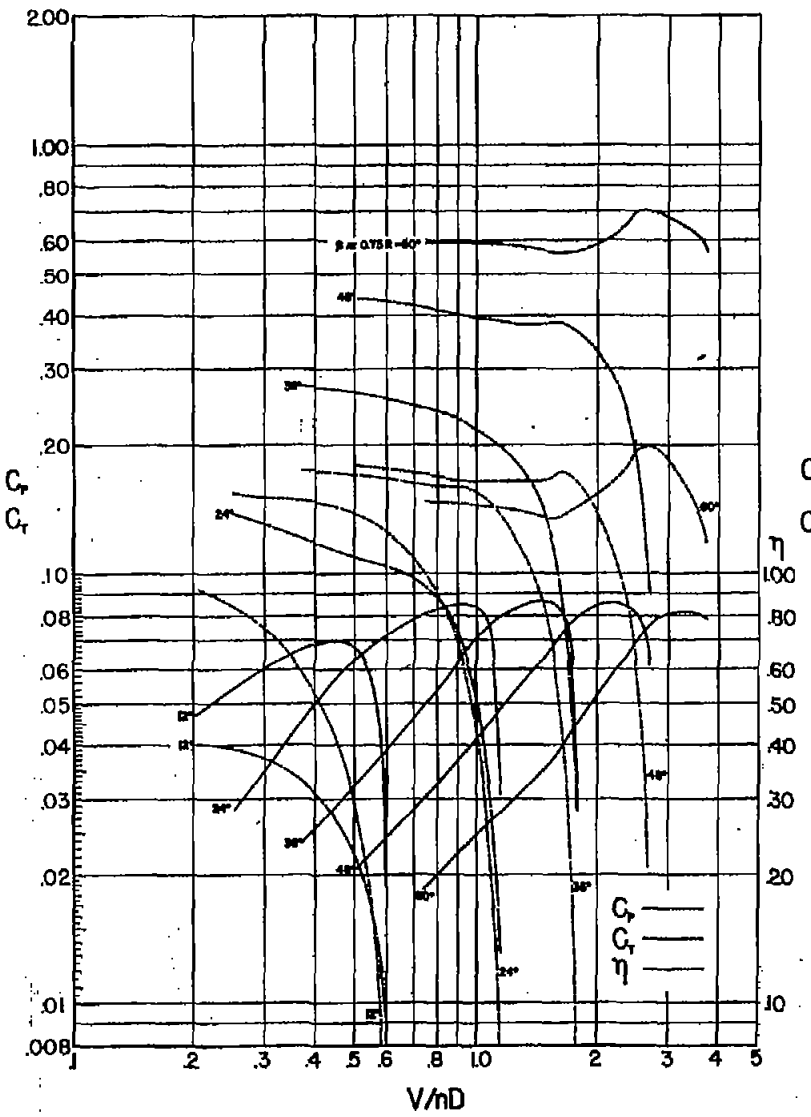

Figure 20.- Characteristics of Model 0.8R.

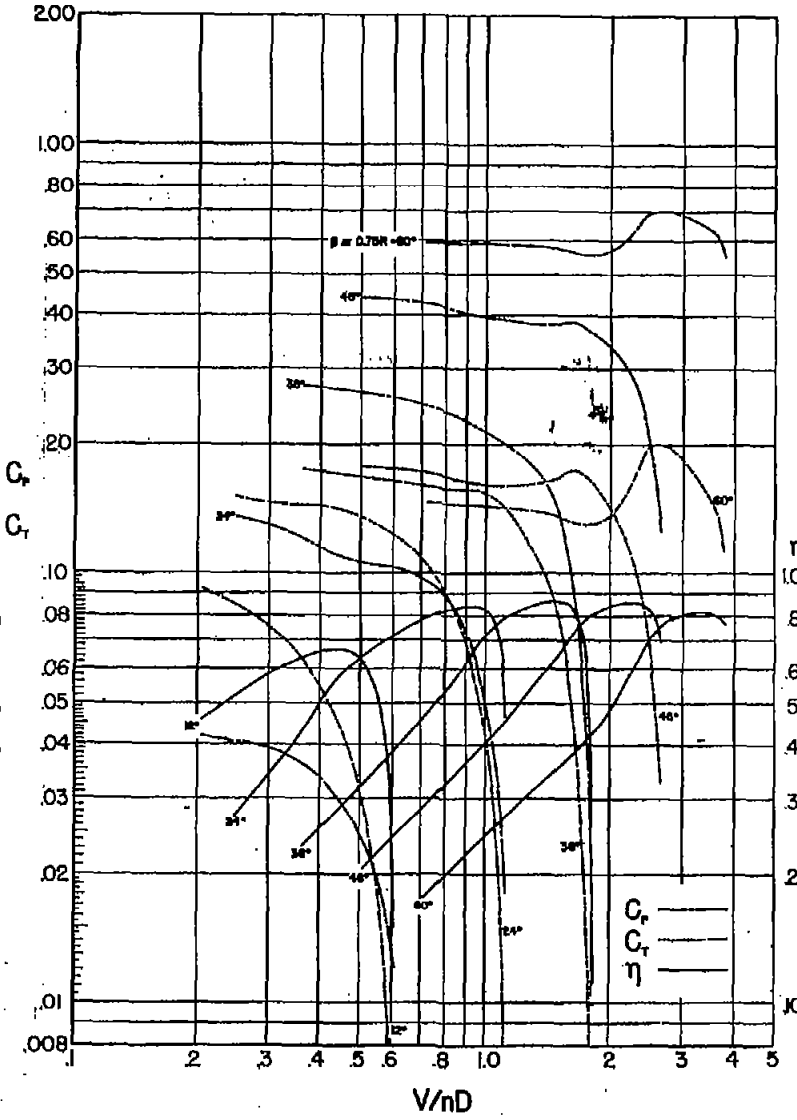

Figure 21.- Characteristics of Model P_{C2} (3 blades).

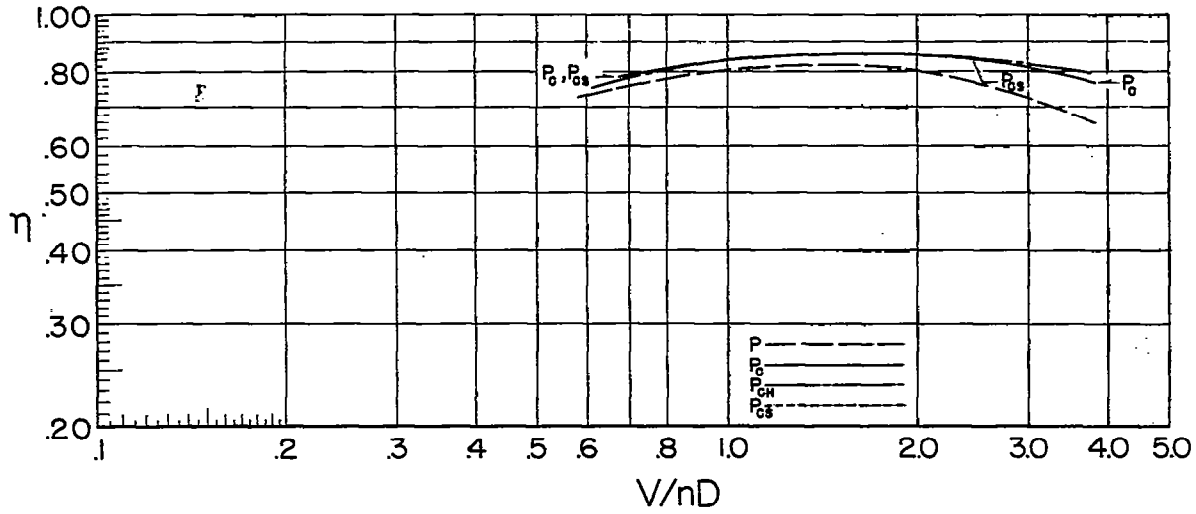

Figure 22.- Efficiency envelopes - thick cuff models.

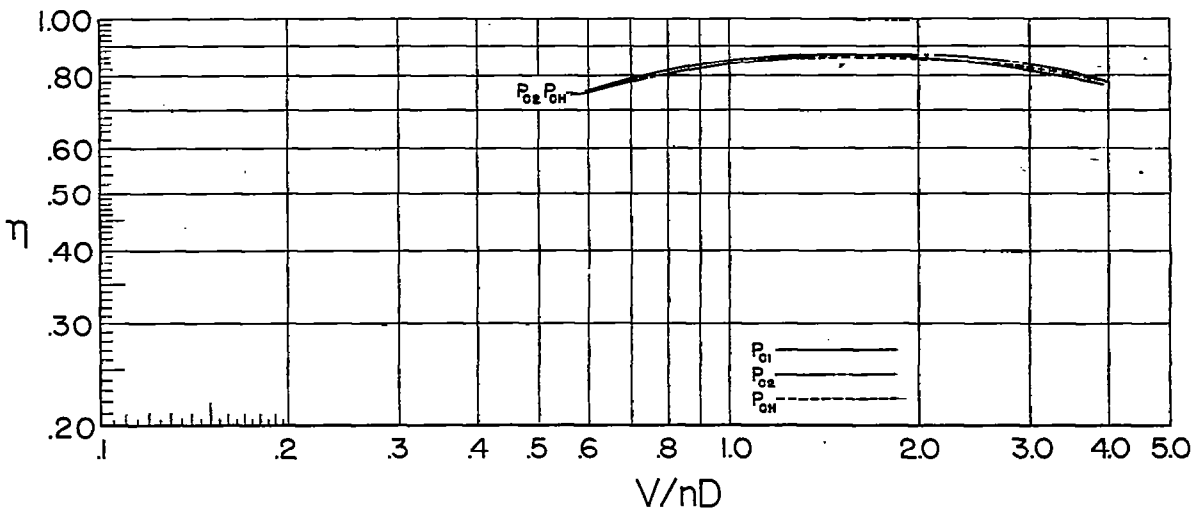

Figure 23.- Efficiency envelopes - thin cuff models (with P_{CH} envelope superimposed).

Figure 24

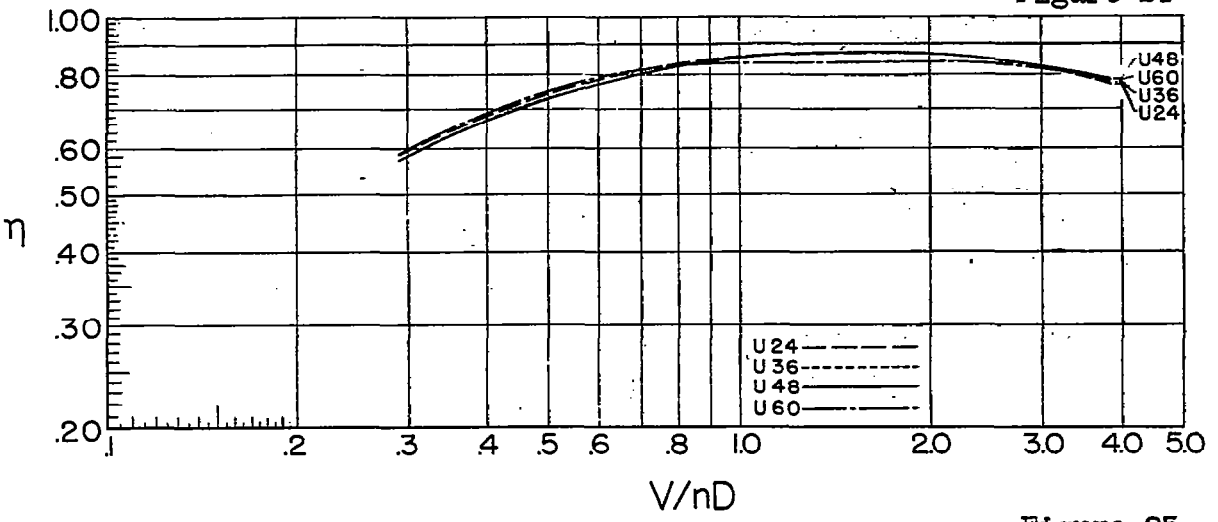

Figure 25

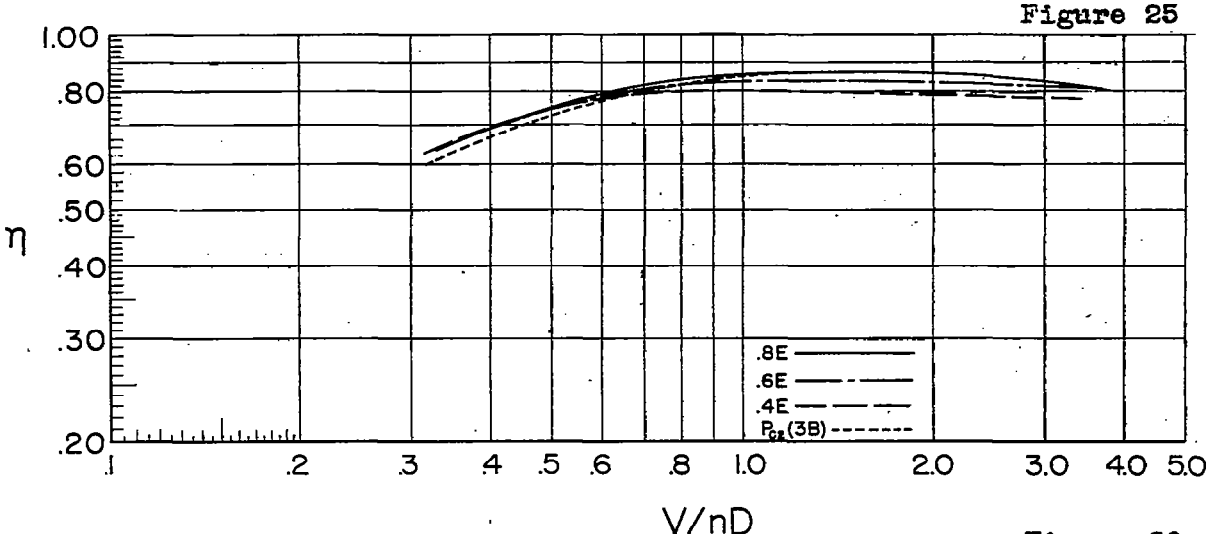

Figure 26

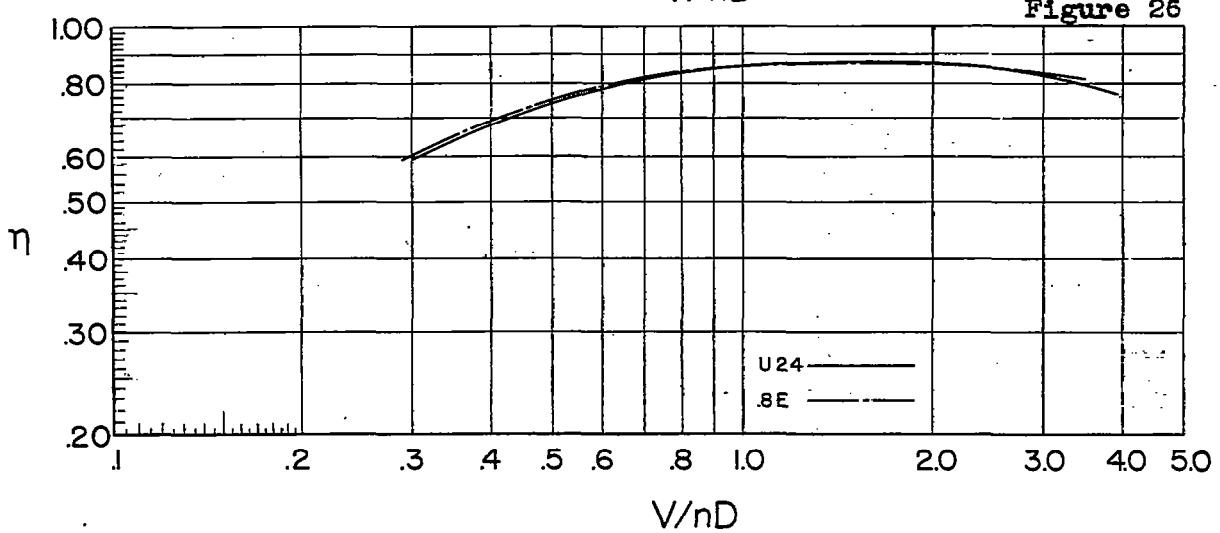

Figures 24, 25, 26.- Efficiency envelopes for models with various distributions of pitch.

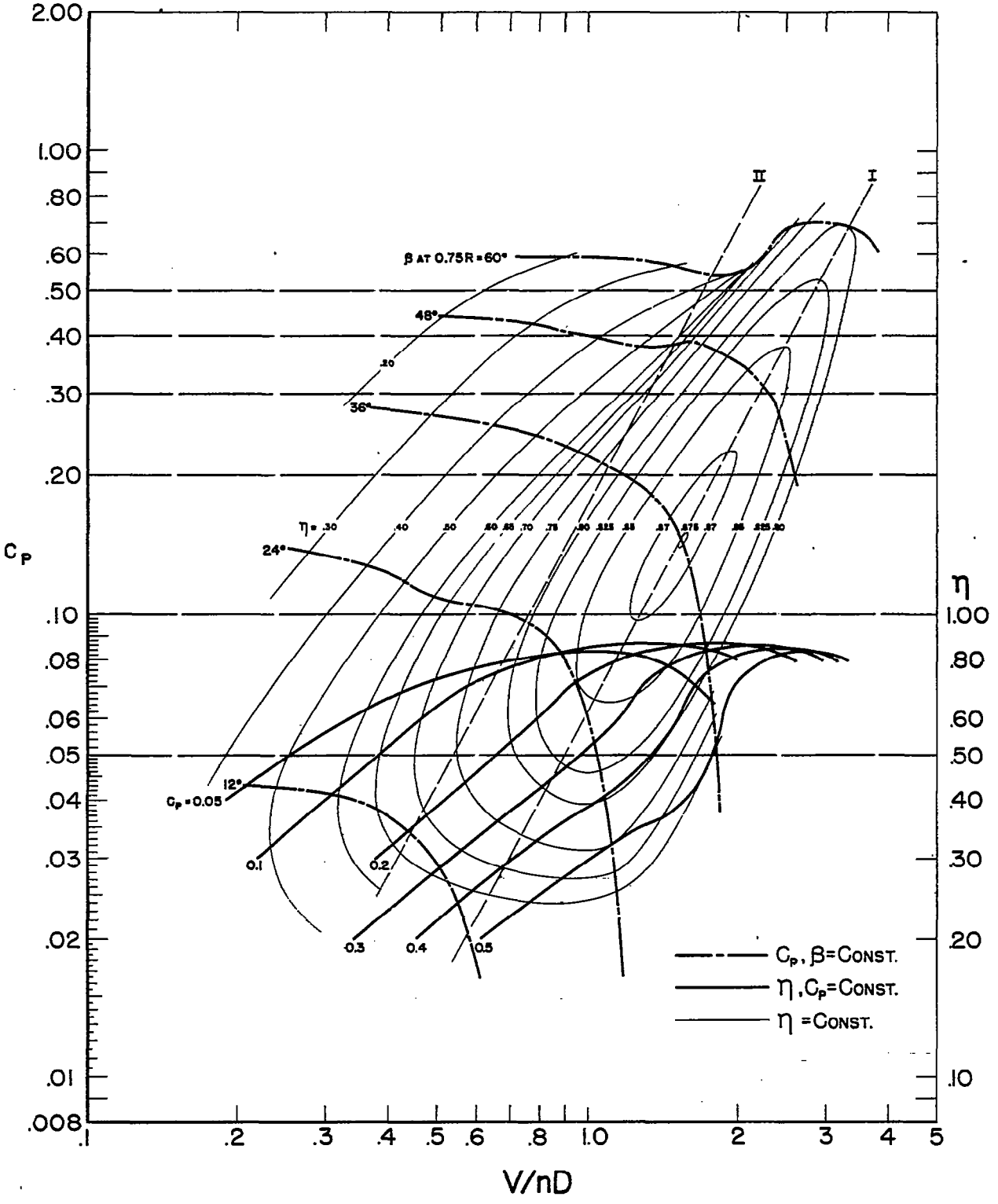

Figure 27.- Construction of constant-speed efficiency curves. (Lines I and II used in subsequent analysis).

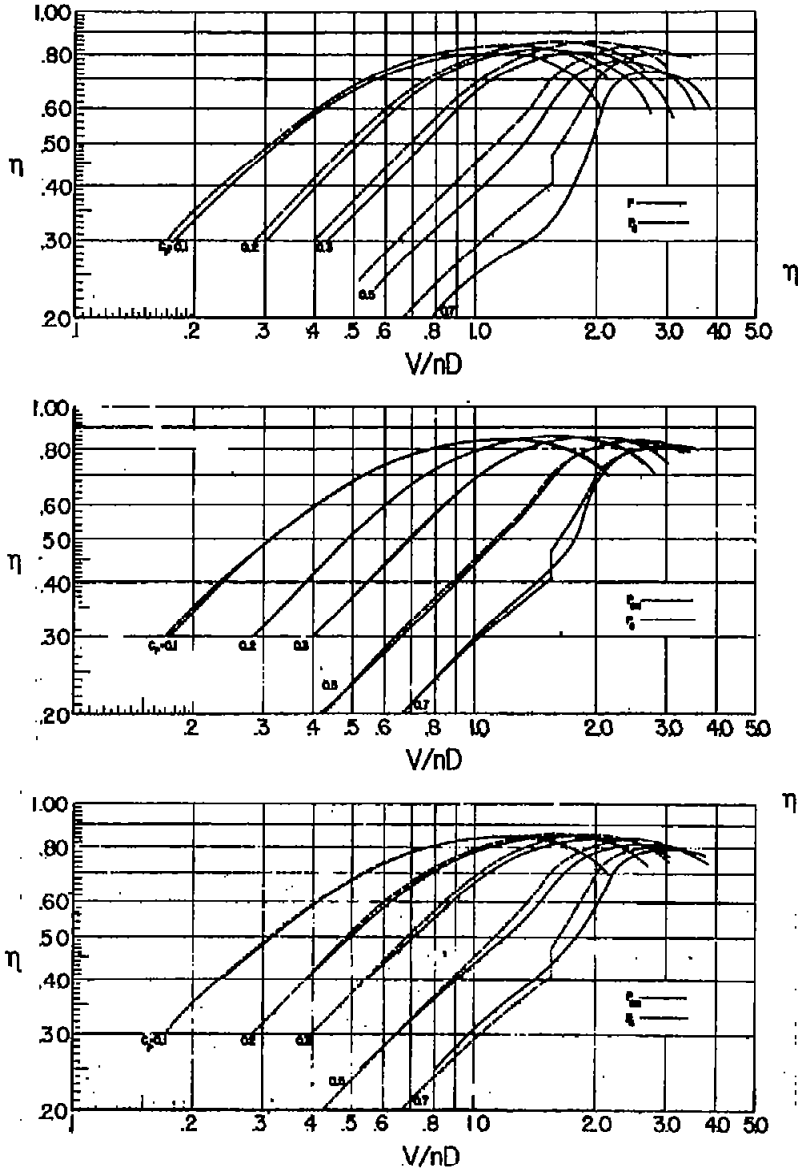

Figure 28.- Constant-speed efficiency curves - thick cuff models.

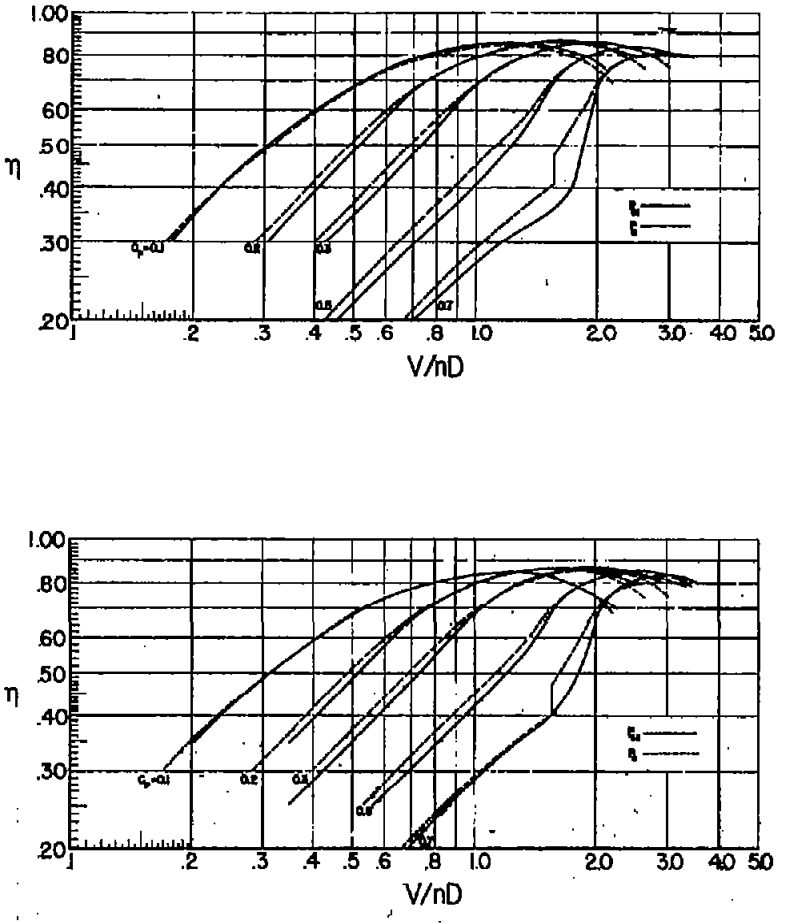

Figure 29.- Constant-speed efficiency curves - thin cuff models. (Compared with thick cuff model P_C).

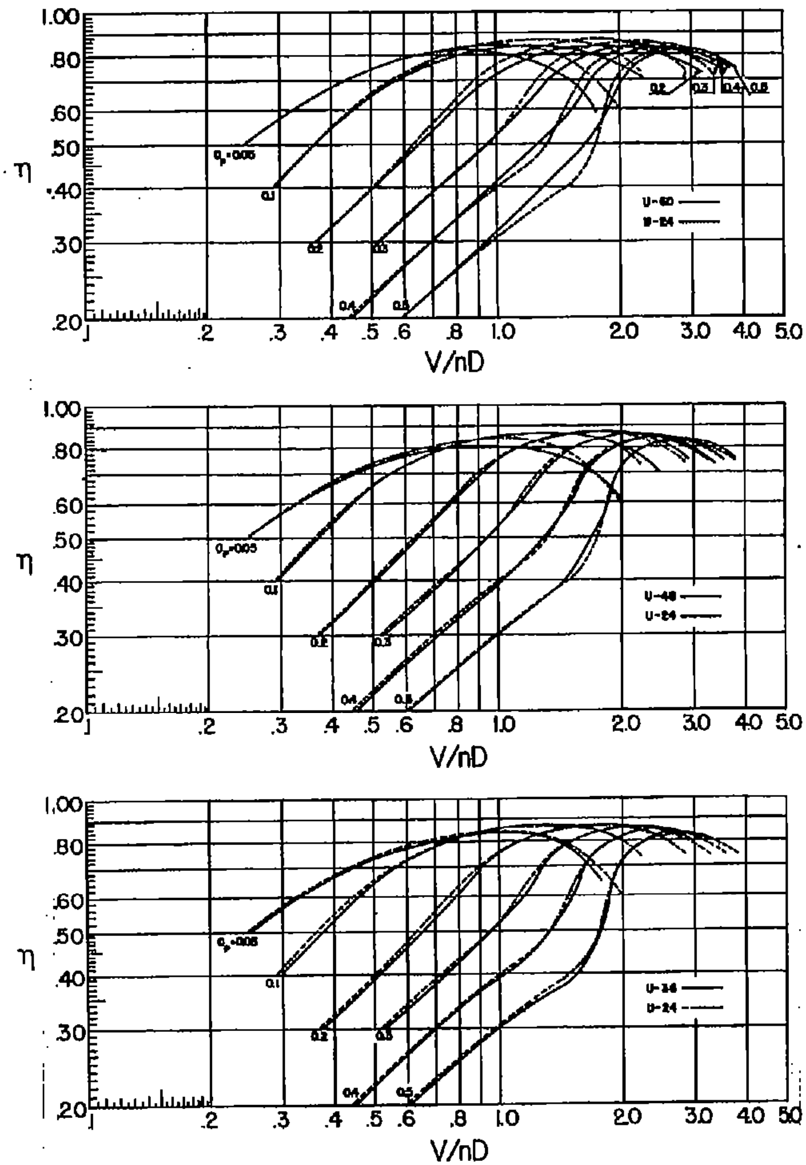

Figure 30.- Constant-speed efficiency curves - uniform pitch models.

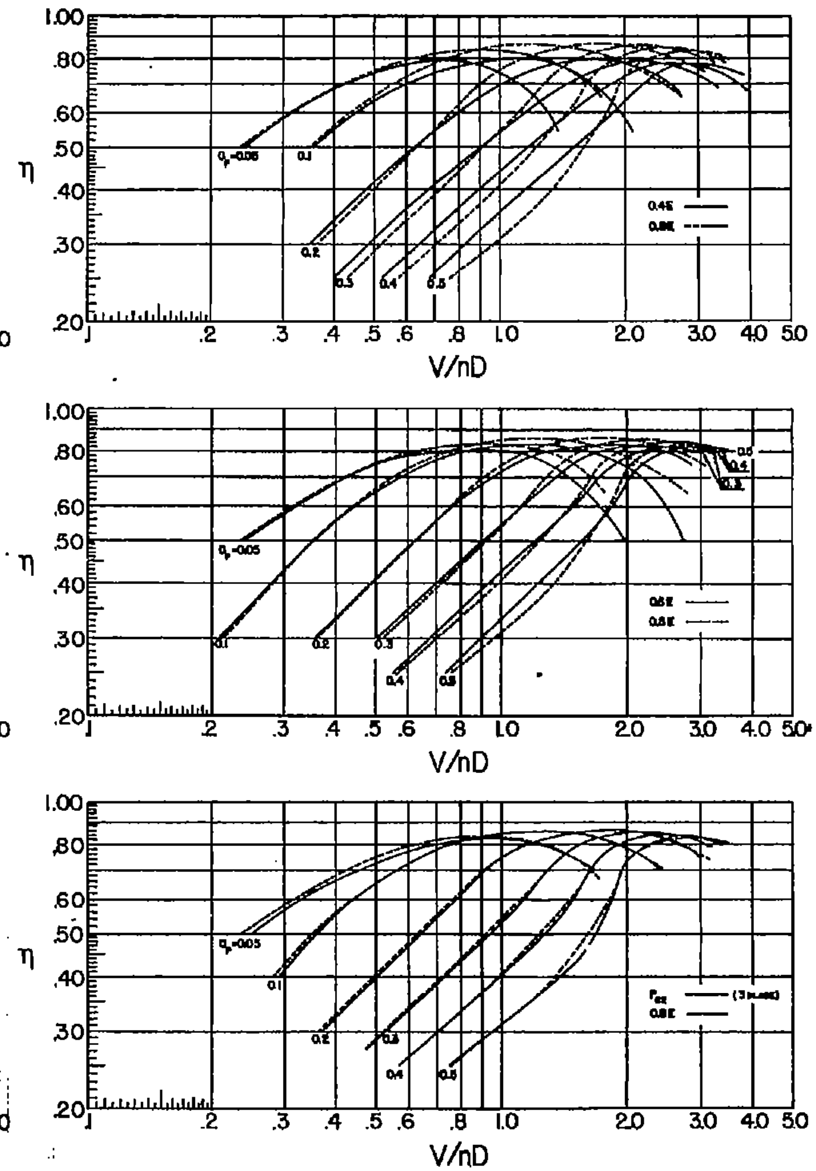

Figure 31.- Constant-speed efficiency curves - non-uniform pitch models.

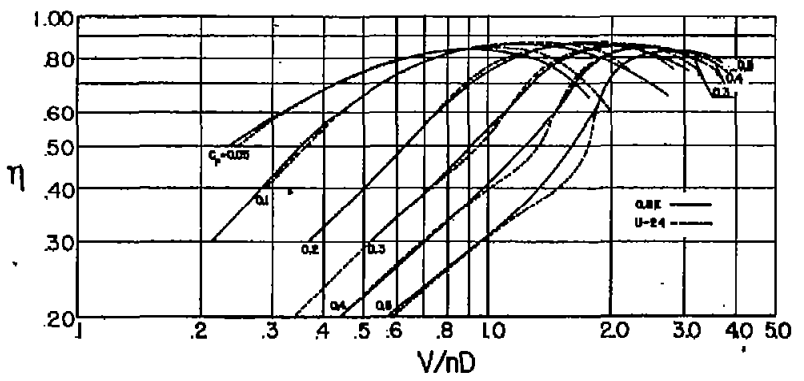

Figure 32.- Comparison of Models U24 and 0.8E.

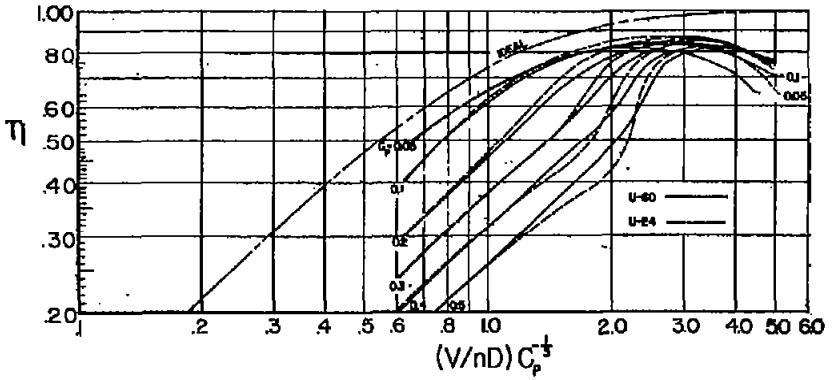

Figure 33.- Ideal and actual efficiencies - large and small uniform design pitch.

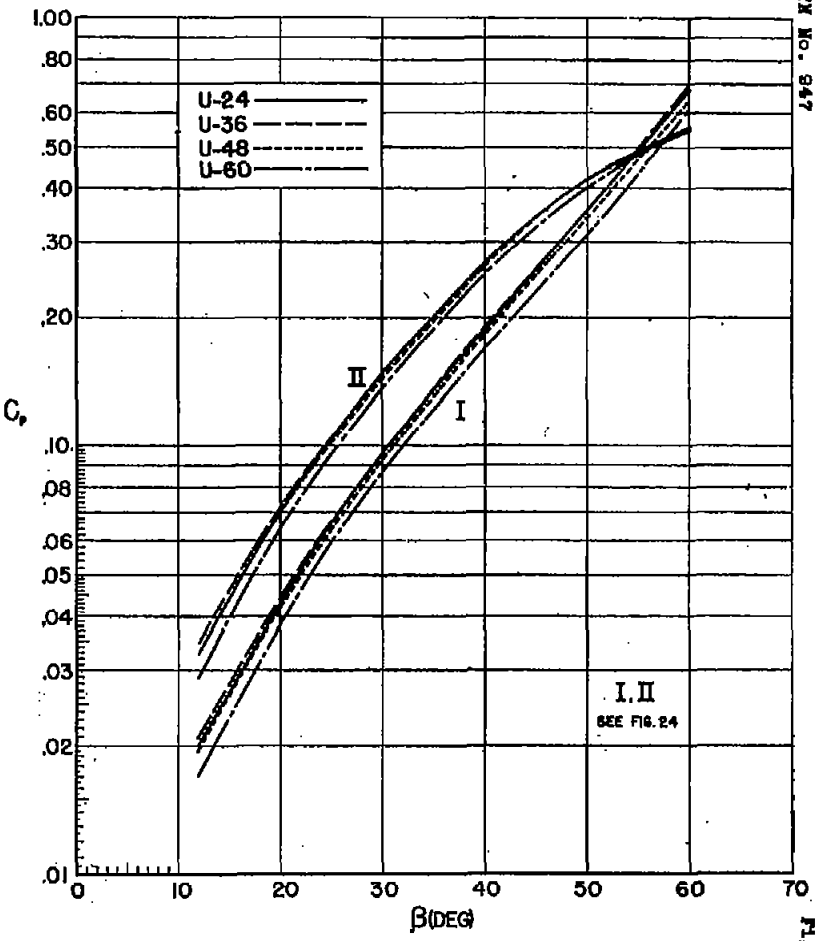

Figure 34.- Power-blade angle relationships - uniform pitch models.

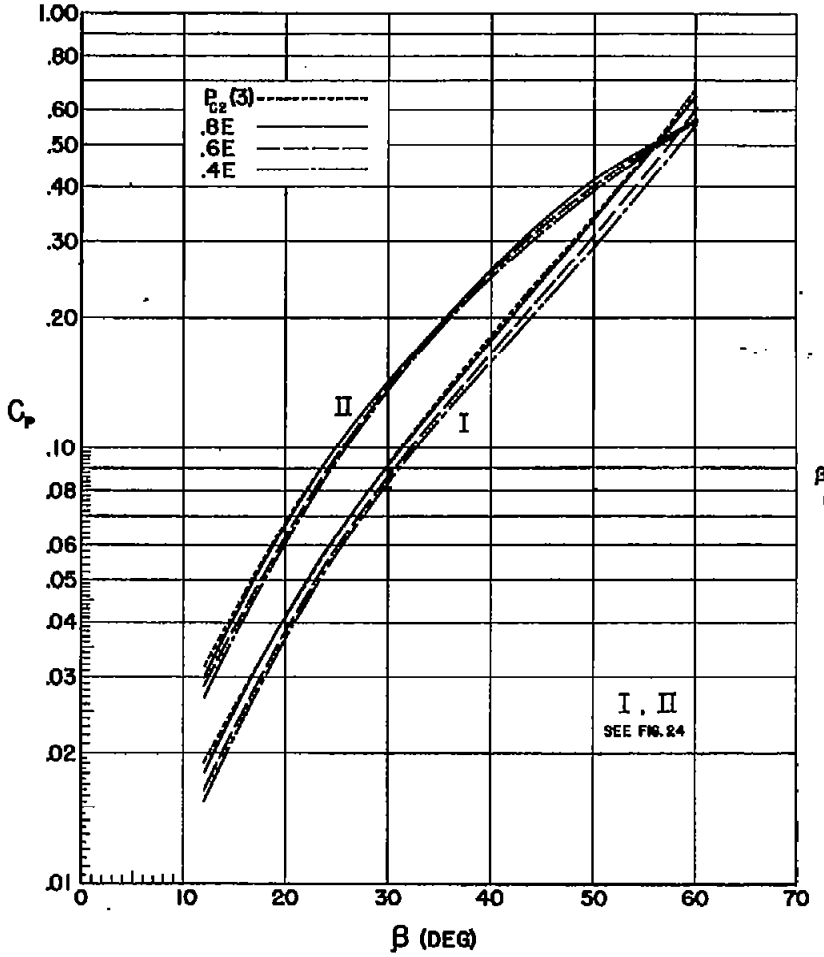

Figure 35.- Power-blade angle relationships - non-uniform pitch models.

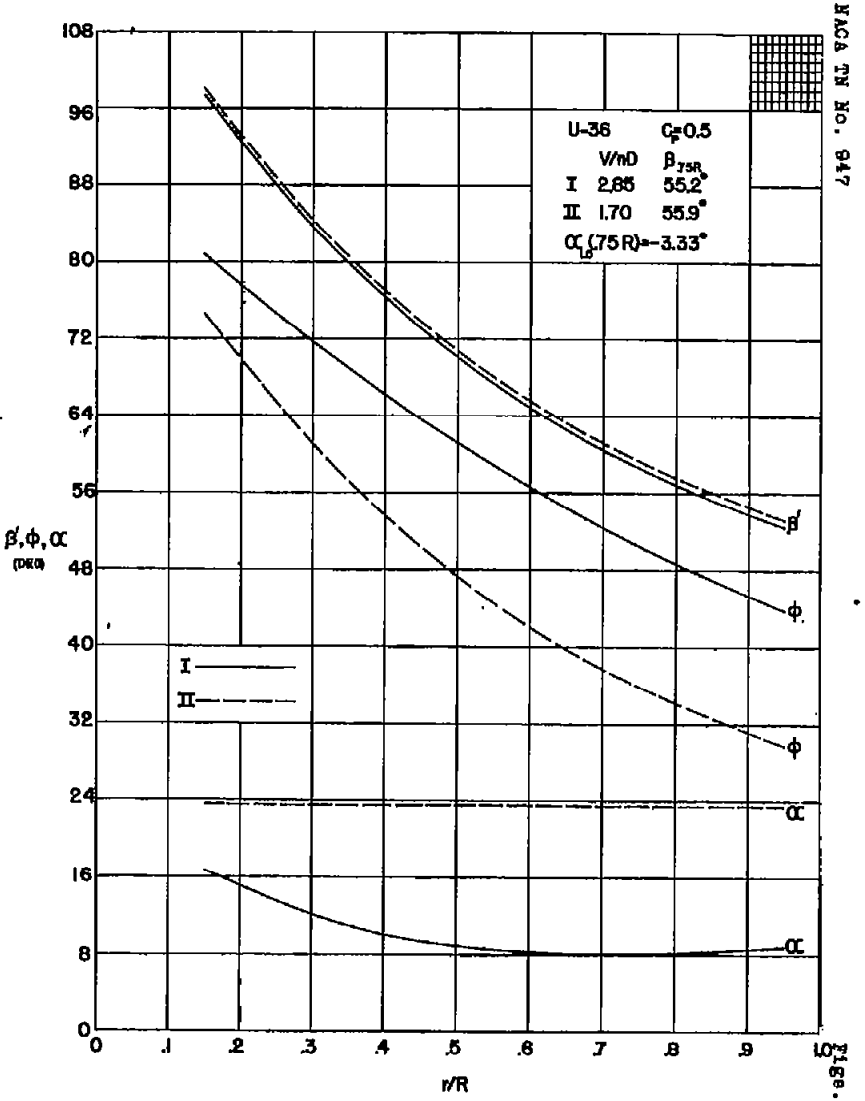

Figure 36.- Sample - Radial distribution of ϕ, β' and α.

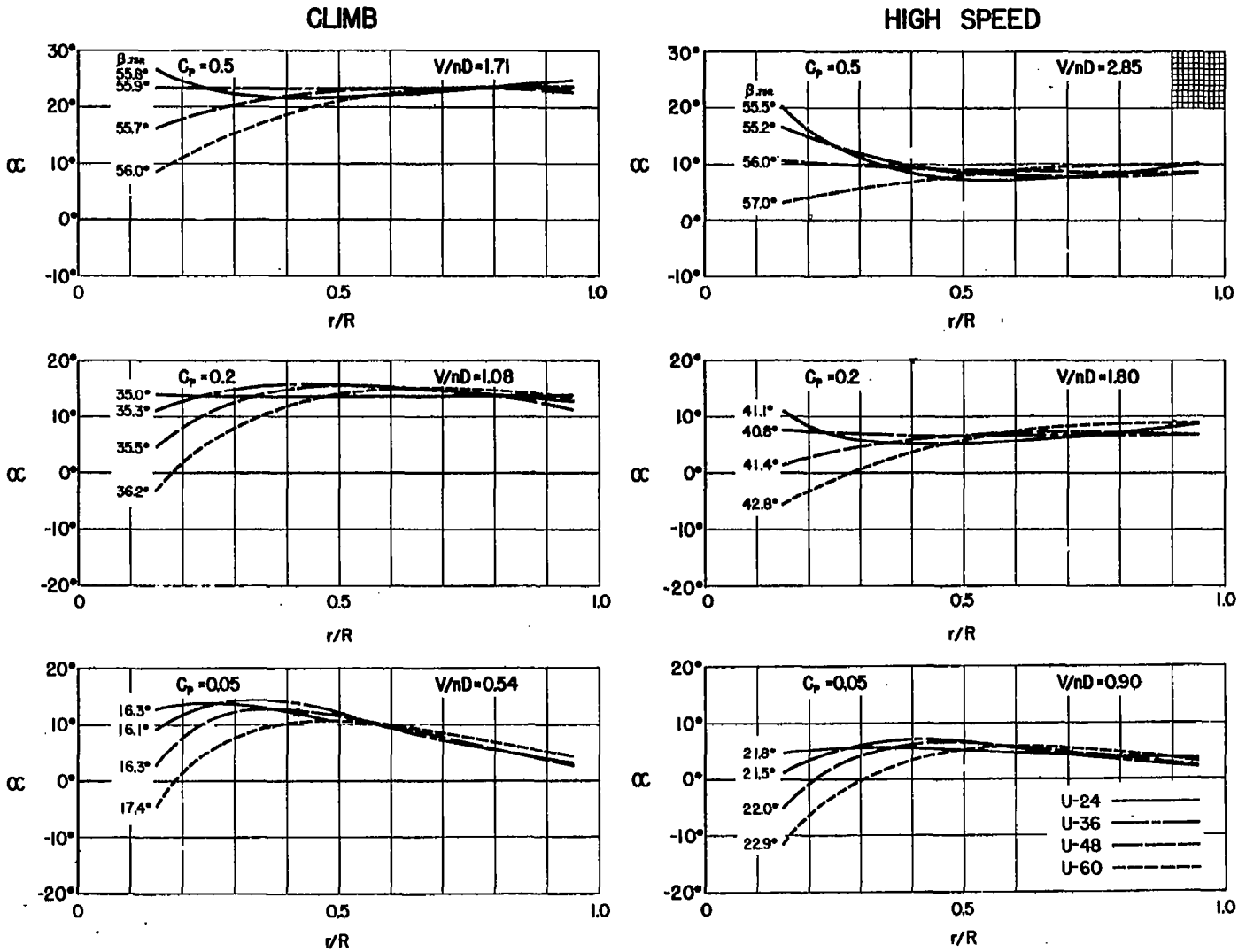

UNIFORM PITCH

Figure 37.- Radial distribution of α for six selected conditions.

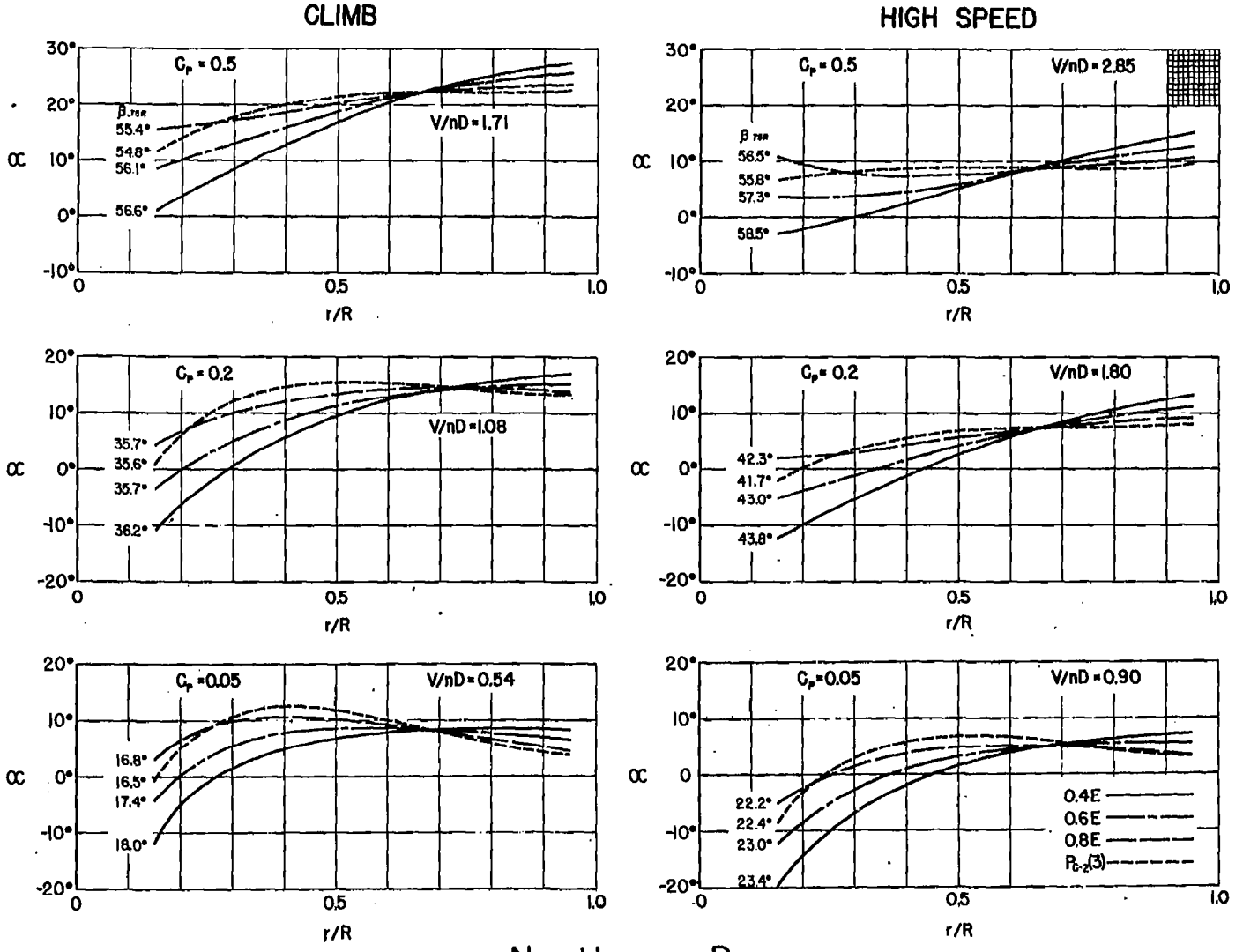

Figure 38.- Radial distribution of α for six selected conditions.

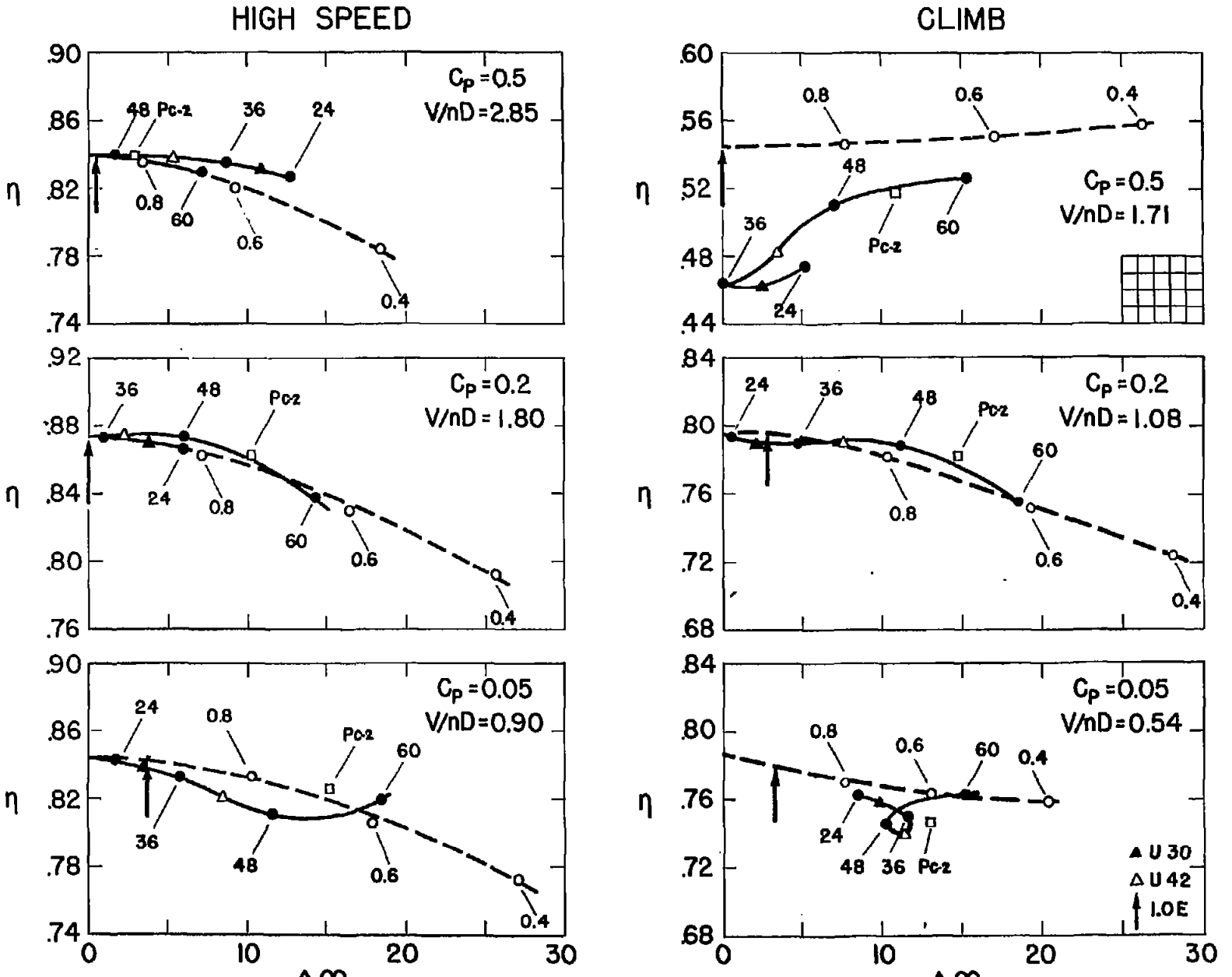

Figure 39.- Variation of η with Δα.

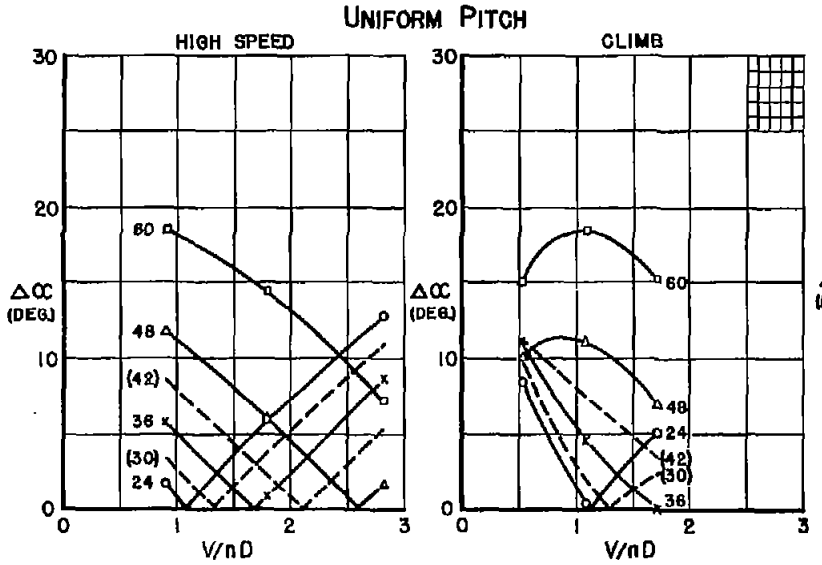

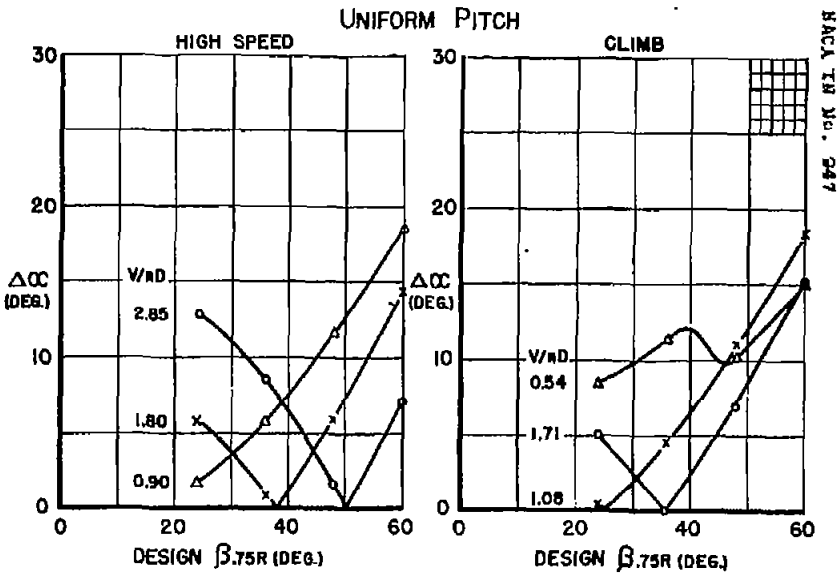

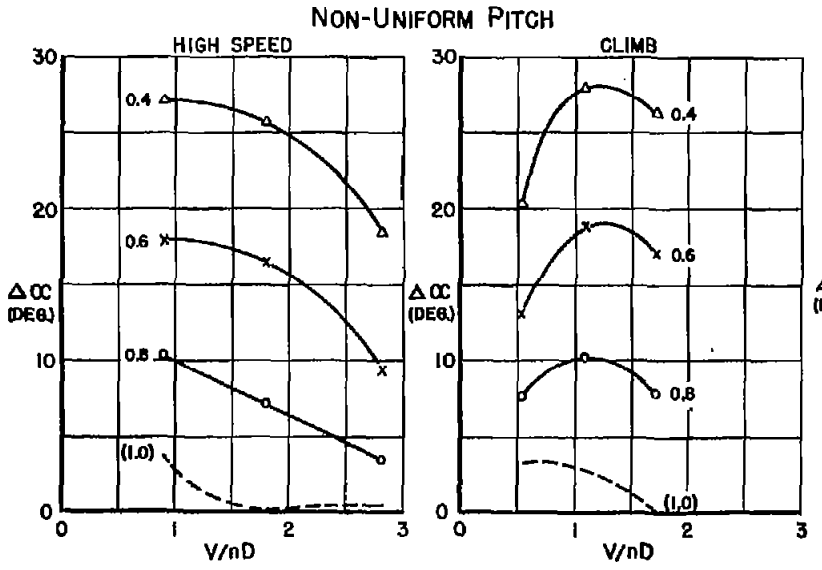

Figure 40.- Variation of $\Delta\alpha$ with V/nD for models with different distributions of pitch.

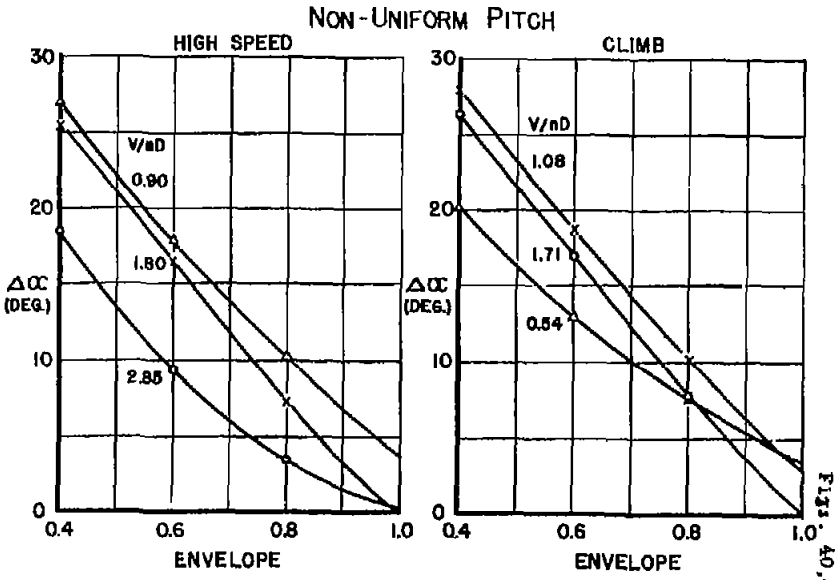

Figure 41.- Variation of $\Delta\alpha$ with design pitch.

Figure 42

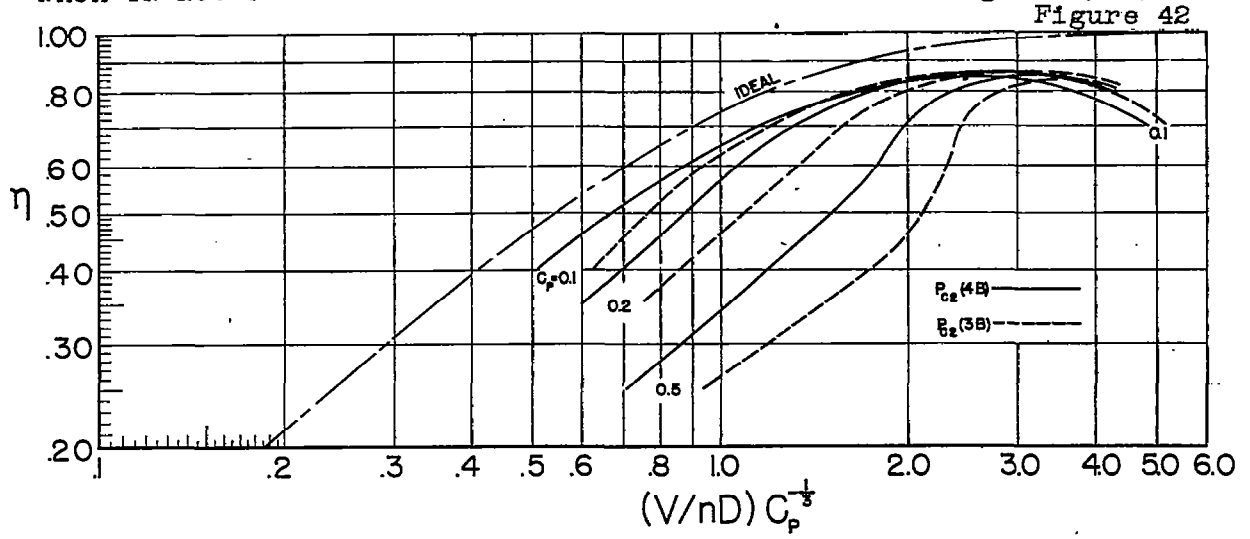

Figure 43

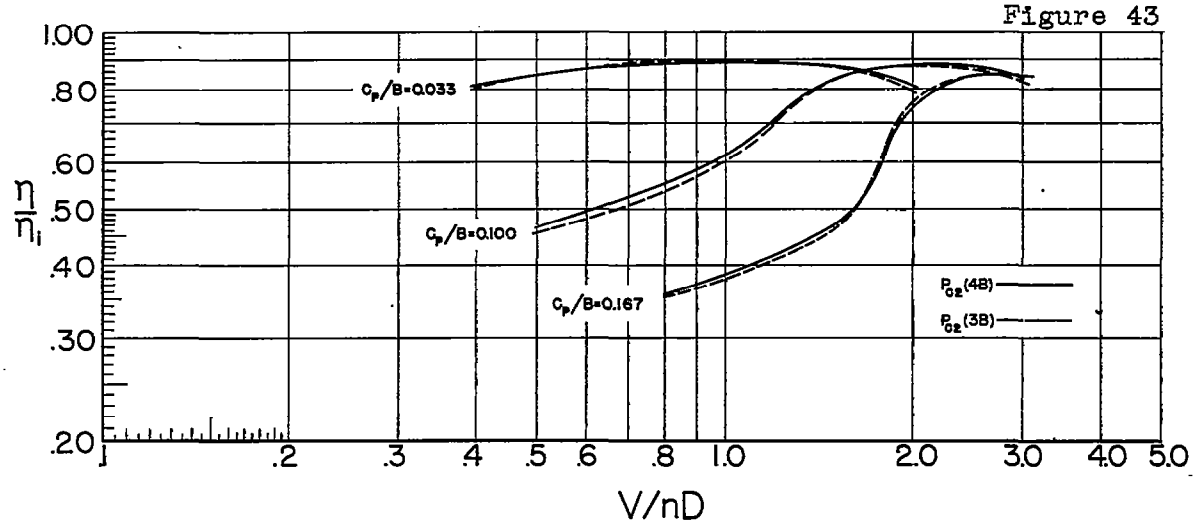

Figure 44

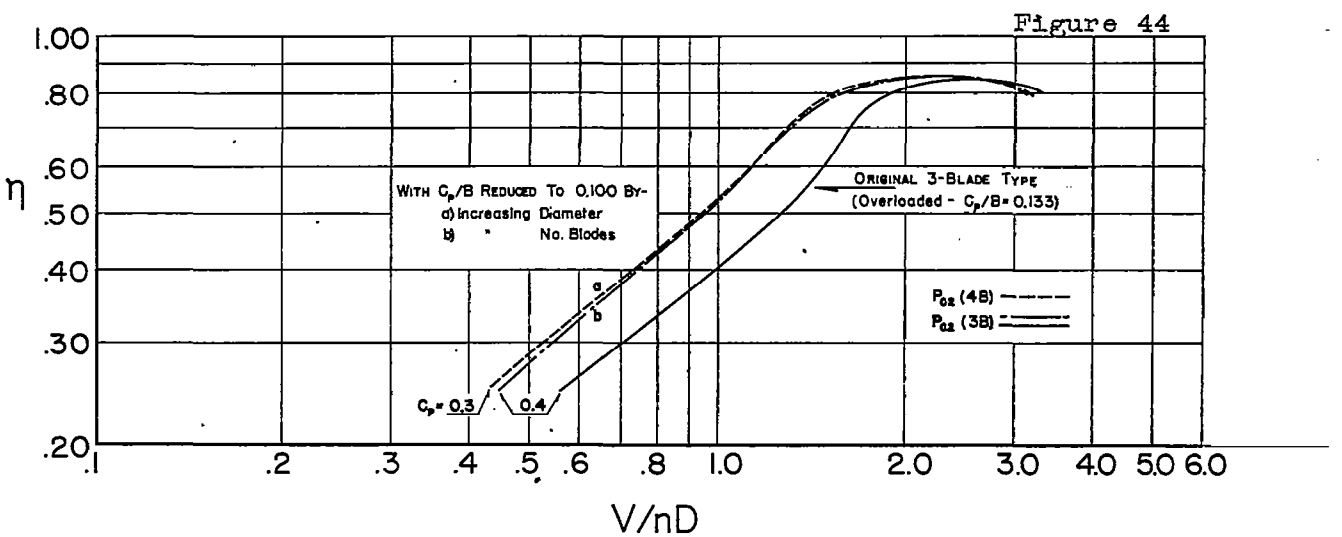

Figures 42, 43, 44.- Effects of blade loading and number of blades upon efficiency.

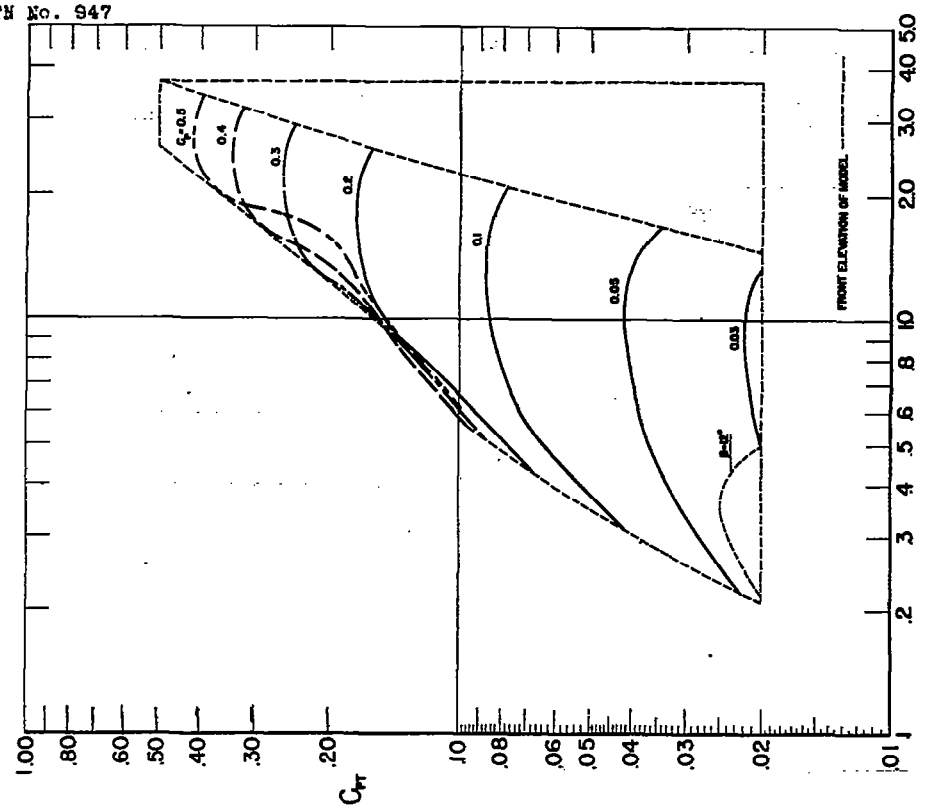

Figure 45.- Profiles of "C_{PT} model" at constant values of C_p

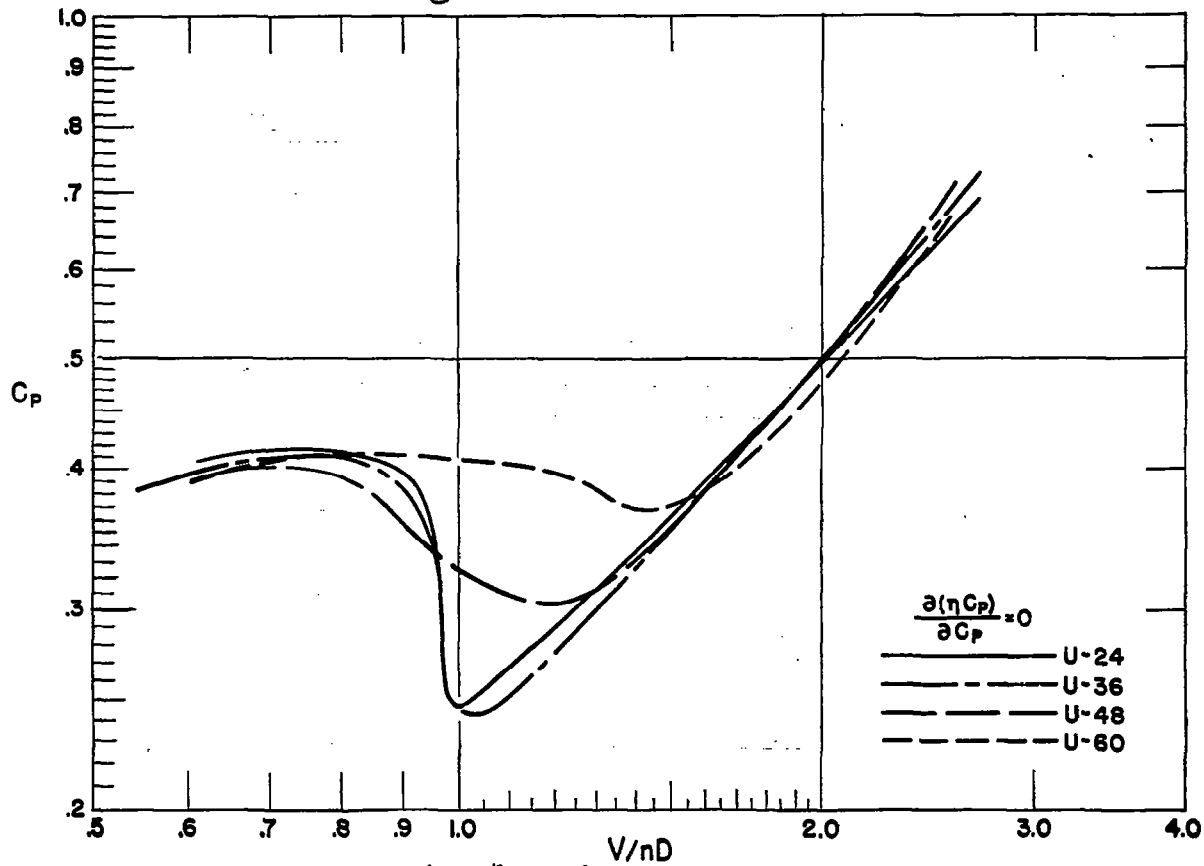

Figure 46.- Crest ($\partial\eta C_p/\partial C_p = 0$) lines - uniform pitch models.

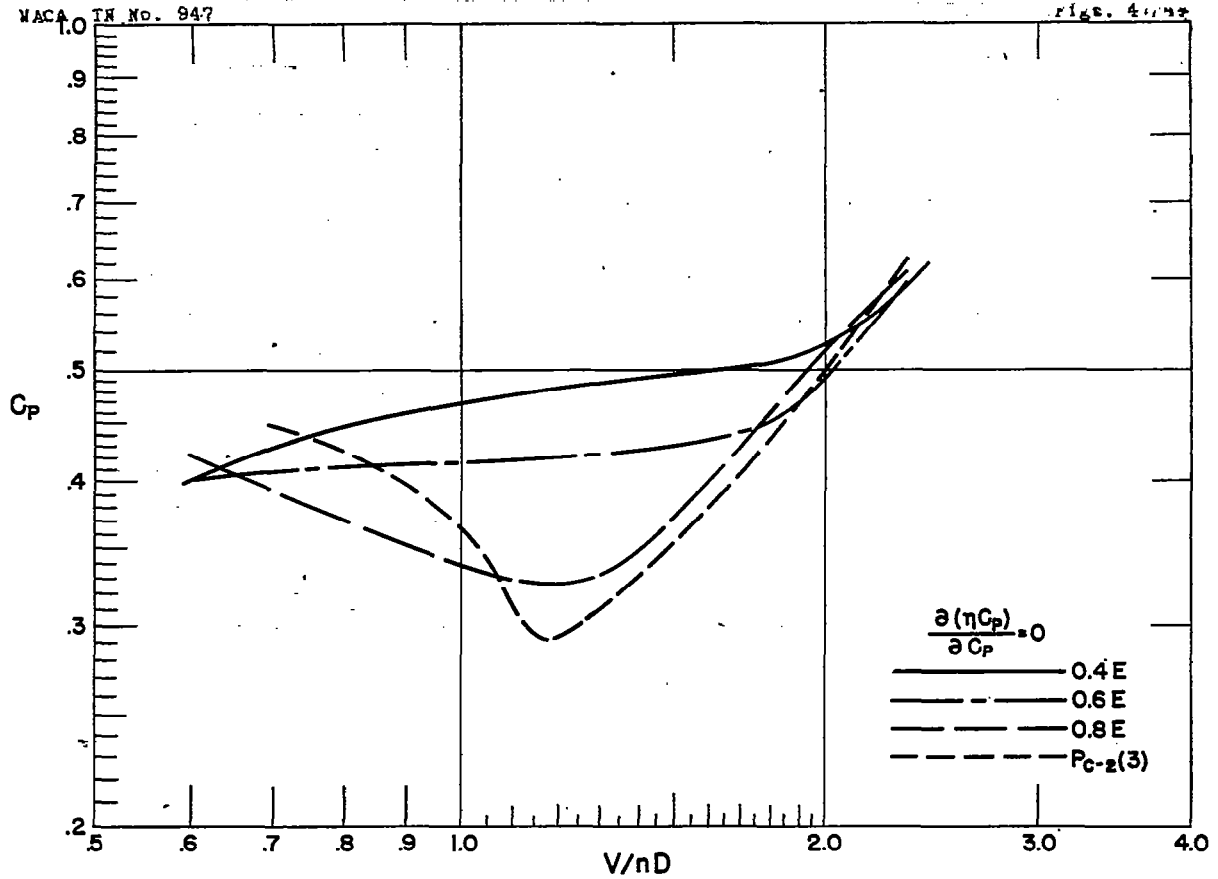

Figure 47.- Crest lines - non-uniform pitch models.

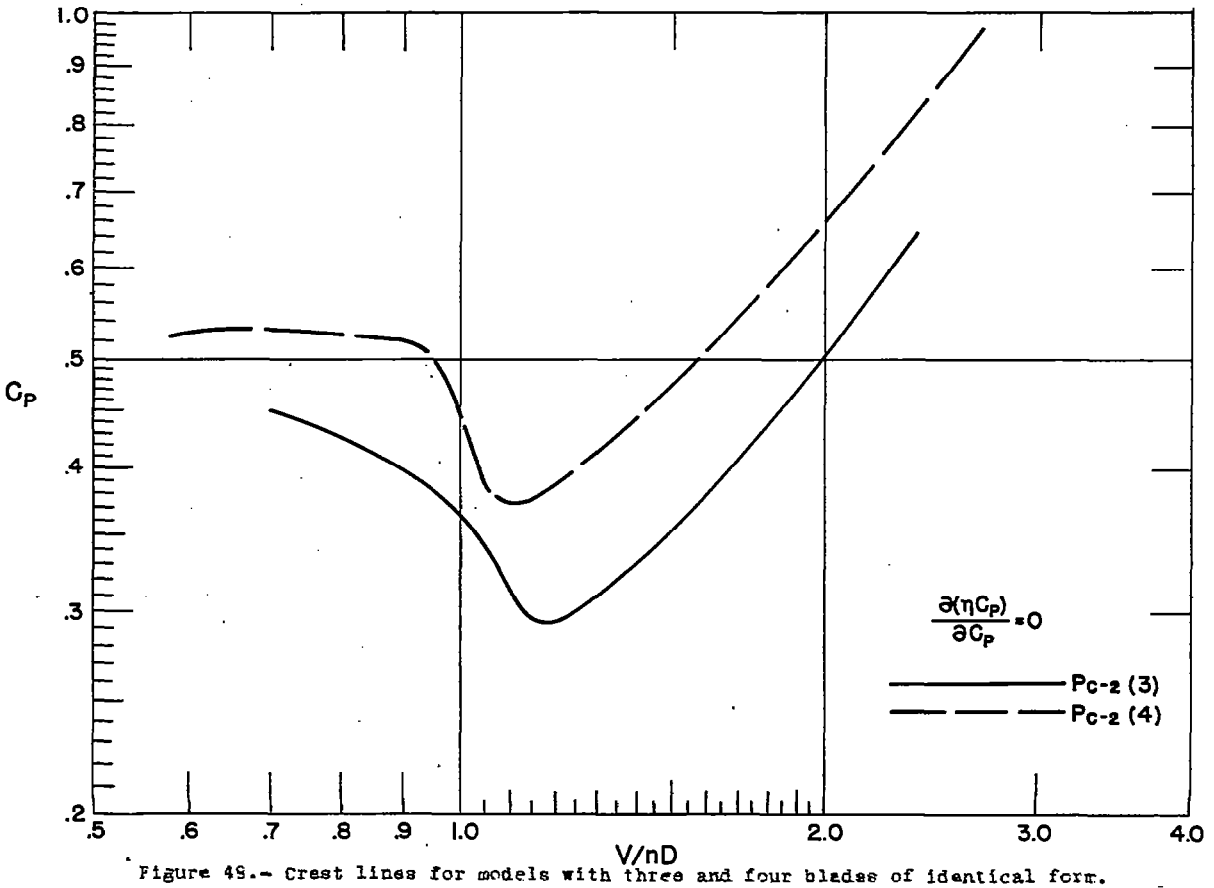

Figure 48.- Crest lines for models with three and four blades of identical form.